



1 Paleo calendar-effect adjustments in time-slice and transient climate- 2 model simulations (PaleoCalAdjust v1.0): impact and strategies for 3 data analysis

4 Patrick J. Bartlein¹, Sarah L. Shafer²

5 ¹Department of Geography, University of Oregon, Eugene, OR 97403, USA

6 ²Geosciences and Environmental Change Science Center, U.S. Geological Survey, Corvallis, OR 97331, USA

7 *Correspondence to:* Patrick J. Bartlein (bartlein@uoregon.edu)

8 **Abstract.** The “paleo calendar effect” is a common expression for the impact that the changes in the length of months or
9 seasons over time, related to changes in the eccentricity of Earth’s orbit and precession, have on the analysis or summarization
10 of climate-model output. This effect can have significant implications for paleoclimate analyses. In particular, using a “fixed-
11 length” definition of months (i.e. defined by a fixed number of days), as opposed to a “fixed-angular” definition (i.e. defined
12 by a fixed number of degrees of the Earth’s orbit), leads to comparisons of data from different positions along the Earth’s orbit
13 when comparing paleo with modern simulations. This effect can impart characteristic spatial patterns or signals in comparisons
14 of time-slice simulations that otherwise might be interpreted in terms of specific paleoclimatic mechanisms, and we provide
15 examples for 6, 97, 116, and 127 ka. The calendar effect is exacerbated in transient climate simulations, where, in addition to
16 spatial or map-pattern effects, it can influence the apparent timing of extrema in individual time series and the characterization
17 of phase relationships among series. We outline an approach for adjusting paleo simulations that have been summarized using
18 a modern fixed-length definition of months and that can also be used for summarizing and comparing data archived as daily
19 data. We describe the implementation of this approach in a set of Fortran 90 programs and modules (PaleoCalAdjust v1.0).

20 1 Introduction

21 There are two ways of defining months or seasons (or any other portion of the year): 1) a “fixed-length” definition, where, for
22 example, months are defined by a fixed number of days (usually those at present), and 2) a “fixed-angular” definition, where,
23 again for example, months are defined by a fixed number of degrees of the Earth’s orbit. Owing to the changes in Earth’s orbit
24 over time these definitions will differ, and comparisons of paleo simulations with modern simulations using a fixed-length
25 definition of months will therefore incorporate data from different positions along the orbit, which can produce patterns in the
26 comparisons that mimic observed paleoclimatic changes. This paleo calendar effect arises from a consequence of Kepler’s
27 second law of planetary motion: Earth moves faster along its elliptical orbit near perihelion, and slower near aphelion. Because
28 the time of year of perihelion and aphelion vary over time, the length of time that it takes the Earth to traverse one-quarter (90
29 degrees) or one-twelfth (30 degrees) of its orbit (a nominal season or month) also varies, so that months or seasons are shorter



30 near perihelion and longer near aphelion. For example, a 30- or 90-degree portion of the orbit will encompass a larger number
31 of days when the Earth is near perihelion (because it is moving faster along its orbit), and a smaller number when it is near
32 aphelion. Likewise, a 30- or 90-day interval will define a shorter orbital arc near perihelion, and a longer one near aphelion.
33 When examining present day and paleo simulations, summarizing data using a fixed-length definition of a particular month
34 (e.g. 31 days of a 365-day year), as opposed to a “fixed-angular” definition (e.g. $(31 \text{ days} / 365.25 \text{ days}) \cdot 360$ degrees of orbit,
35 where 365.25 is the number of days in a year), will therefore result in comparing conditions that prevailed over different
36 portions of the Earth’s orbit. Consequently, comparisons of present-day and paleoclimatic simulations that use the same
37 calendar (e.g. a present-day fixed-length calendar definition of January as 31-days long) will include two components of
38 change, one consisting of the actual model-simulated climate change between the present and paleo time period, and a second
39 arising simply from the difference in the angular portion of the orbit defined by 31 days at present as opposed to 31 days at the
40 paleo time period.

41 This impact of the calendar effect on the analysis of paleoclimatic simulations and their comparison with present-day or
42 “control” simulations is well known and not trivial (e.g. Kutzbach and Gallimore, 1988; Joussaume and Braconnot, 1997).
43 The effect is large and spatially variable, and can produce apparent map patterns that might otherwise be interpreted as evidence
44 of, for example, latitudinal amplification or damping of temperature changes, development of continental/marine temperature
45 contrasts, interhemispheric contrasts (the “bipolar seesaw”), changes in the latitude of the intertropical convergence zone
46 (ITCZ), variations in strength of the global monsoon, and others. In transient climate-model simulations, time series of data
47 aggregated using a fixed modern calendar, as opposed to an appropriately changing one, can differ not only in the overall shape
48 of long-term trends in the series, but also in variations in the timing of, for example, Holocene “thermal maxima” which,
49 depending on the time of year, can be on the order of several thousand years. The impact arises not only from the orbitally
50 controlled changes in insolation amount and the length of months or seasons, but also from the advancement or delay in the
51 starting and ending days of months or seasons relative to the solstices. Even if daily data are available, the calendar effect
52 must still be considered when summarizing those data by months or seasons, or when calculating climatic indices such as the
53 mean temperature of the warmest or coldest calendar month—values that are often used for comparisons with paleoclimatic
54 observations (e.g. Harrison et al., 2014, and see Kageyama et al., 2018, for further discussion). It is also the case that the
55 calendar effect can have a small impact on annual-average values, because the first day of the first month of the year may fall
56 in the previous year, and the last day of the last month of the year may fall in the next year.

57 Various approaches have been proposed for incorporating the calendar effect or “adjusting” monthly values in analyses of
58 paleoclimatic simulations (e.g. Pollard and Reusch, 2002; Timm et al., 2008; Chen et al., 2011). Despite this work, the calendar
59 effect is generally ignored, and so our motivation here is to provide an adjustment method that is relatively simple and can be
60 applied generally to “CMIP-formatted” (<https://esgf-node.llnl.gov/projects/cmip5/>) files, such as those distributed by the
61 Paleoclimate Modelling Intercomparison Project (PMIP, Kageyama et al., 2018). Our approach (broadly similar to Pollard



62 and Reusch, 2002) involves (1) determining the appropriate fixed-angular month lengths for a paleo experiment (e.g., Kutzbach
63 and Gallimore, 1988), (2) interpolating the data to a daily time step using a mean-preserving interpolation method (e.g.,
64 Epstein, 1991), and then (3) averaging or accumulating the interpolated daily data using the appropriate (paleo) month starting
65 and ending days, thereby explicitly incorporating the changing month lengths. In cases where daily data are available (e.g. in
66 CMIP5/PMIP3 “day” files), only the third step is necessary. This approach is implemented in a set of Fortran 90 programs
67 and modules (PaleoCalAdj v1.0, described below). With a suitable program code “wrapper” file, the approach can also be
68 applied to transient simulations (e.g. Liu et al., 2009; Ivanovic et al., 2016).

69 In the following discussion, we describe (a) the calendar effect on month lengths and their beginning, middle and ending days
70 over the past 150 kyr; (b) the spatial patterns of the calendar effect on temperature and precipitation rate for several key times
71 (6, 97, 116, and 127 ka); and (c) the methods that can be used to calculate month lengths (on various calendars) and to “calendar
72 adjust” monthly or daily paleo model output to an appropriate paleo calendar.

73 **2 Month-length variations**

74 The fixed-angular length of months as they vary over time can be calculated using the algorithm in Appendix A of Kutzbach
75 and Gallimore (1988). This algorithm yields the length of time (in real-number or fractional days) required to traverse a given
76 number of degrees of celestial (as opposed to geographical) longitude starting from the vernal equinox, the common “origin”
77 for orbital calculations (see Jousaume and Braconnot, 1997, for discussion). Although developed for a 360-day year with
78 30-day months at present, the algorithm can easily be adapted for other calendars and for cases where the present-day months
79 are not equal in length. The beginnings and ends of each fixed-angular month in a 365-day “no-leap” calendar are shown at 1
80 kyr intervals for the past 150 kyr in Fig. 1, calculated using the approach described in Sects. 4.2-4.5 below. (See section 4.4.1
81 of the *NetCDF Climate and Forecast Metadata Conventions* (<http://cfconventions.org/>) for a discussion of climate-model
82 output calendar types.) The month-length “anomalies” (i.e. long-term differences between paleo and present month lengths,
83 with present defined as 1950 CE) are shown in color, with (paleo) months that are shorter than those at present in green shades,
84 and months that are longer than those at present in blue shades. Not only do the lengths of fixed-angular months vary over
85 time, but so do their middle, beginning and ending days (Fig. 2), with mid-month days that are closer to the June solstice
86 indicated in orange and those that are farther from the June solstice in blue. The variations in month length (Fig. 1) obviously
87 track the changing time of year of perihelion, while the beginning and ending day anomalies reflect the climatic precession
88 parameter (Fig. 2). The shift in the beginning, middle, or end of individual months relative to the solstices ultimately controls
89 the average or mid-month daily insolation at different latitudes (Figs. 3-5). The calendar effect is illustrated below for four
90 times: 6 and 127 ka are the target times for the planned warm-interval *midHolocene* and *lig127k* CMIP6/PMIP4 (Coupled
91 Model Intercomparison Project Phase 6/Paleoclimate Modelling Intercomparison Project Phase 4) simulations (Otto-Bliesner
92 et al., 2017) and illustrate the calendar effects when perihelion occurs in the boreal summer or autumn (Fig. 6); 116 ka is the



93 time of a proposed sensitivity experiment for the onset of glaciation (Otto-Bliesner et al., 2017), and illustrates the calendar
94 effect when perihelion occurs in boreal winter; and 97 ka was chosen to illustrate an orbital configuration not represented by
95 the other times (i.e. one with boreal spring months occurring closer to the June solstice).

96 At 6 ka, perihelion occurred in September (Fig. 6), and the months from May through October were shorter than today (Fig.
97 1), with the greatest differences in August (1.65 days shorter than present). This contraction of month lengths moved the
98 middle of all of the months from April through December closer to the June solstice (Fig. 2), with the greatest difference in
99 November (4.9 days closer to the June solstice, and so 4.9 days farther from the December solstice). At 127 ka, perihelion
100 was in late June, and the months April through September were shorter than today (Fig. 1), with the greatest difference in July
101 (3.23 days shorter than present). As at 6 ka, the shorter boreal summer months move the middle of the months between July
102 and December closer to the June solstice (Fig. 2), with the greatest difference in September and October (12.4 and 12.3 days
103 closer, respectively). At both 6 and 127 ka, the longer boreal winter months begin and end earlier in the year, placing the
104 middle of January 3.3 (6 ka) and 4.3 (127 ka) days farther from the June solstice than at present. As can be noted on Figs. 1
105 and 2, 127 ka does not represent a simple amplification of 6 ka conditions. Although broadly similar in having shorter late
106 boreal summer and autumn months that begin earlier in the year (and hence closer to the June solstice), the two times are only
107 similar in the relative differences from present in month length and beginning and ending days.

108 At 116 ka, perihelion was in late December, and consequently the months from October through March were shorter than
109 present (Fig. 1). This has the main effect of moving the middle of the months July through December farther from the June
110 solstice (with a maximum in September of 5.6 days; Fig. 2), somewhat opposite to the pattern at 6 and 127 ka. At 97 ka,
111 perihelion occurred in mid-November, in between its occurrence in September at 6 ka and December at 116 ka (Fig. 1). The
112 impact on month length and mid-month timing is complicated, with the mid-month days of January through March and July
113 through October occurring farther from the June solstice (Fig. 2).

114 The first-order impact of the calendar effect can be gauged by comparing (at a particular latitude) daily insolation values for
115 mid-month days determined using the appropriate paleo calendar (which assumes fixed-angular definitions of months) with
116 insolation values for mid-month days using the present-day calendar (which assumes fixed-length definitions of months). At
117 6 ka, at 45° N, the shorter (than present), and earlier (relative to the June solstice) months of September through November
118 had insolation values over 10 W m⁻² greater for mid-month days defined using the fixed-angular paleo calendar, in comparison
119 with values determined using the fixed-length present-day calendar (Fig. 3), and at 127 ka, the differences exceeded 35 W m⁻²
120 for the months of August through October. These positive insolation differences were accompanied by negative differences
121 from January through June. At first glance, it may be counterintuitive that the calendar effects that yield positive differences
122 in mid-month insolation are not balanced by the negative insolation differences as is the case with the month-length differences.
123 However, the calendar effects on insolation include both the month-length differences as well as long-term insolation



124 differences themselves (Figs. 7-9), which are not symmetrical within the year, and so the calendar effects do not “cancel out”
125 within the year.

126 At 116 ka, the longer but later occurring month of September had a negative difference in mid-month insolation that exceeded
127 10 W m^{-2} . For regions where surface temperatures are strongly tied to insolation with little lag, such as the interiors of the
128 northern continents, these calendar effects on insolation will directly be reflected by the calendar effects on temperatures. By
129 moving the beginning, middle and end of individual months (and seasons) closer to or farther from the solstices, the “apparent
130 temperature” of those intervals will be affected (i.e. months or seasons that start or end closer to the summer solstice will be
131 warmer). The calendar effect on insolation varies strongly with latitude, with the sign of the difference broadly reversing in
132 the southern hemisphere (Figs. 3-5).

133 **3 Impact of the calendar effect**

134 Past demonstrations of the calendar effect have used “real” paleoclimatic simulations, and so the climate patterns being used
135 in these demonstrations include both the calendar effect, and the long-term mean differences in climate between experiment
136 and control simulations. Comparison of Figs. 3 and 7 clearly shows, however, that the variations over time in insolation and
137 in the calendar effect are not identical, and so the use of an actual paleoclimatic experiment (e.g. for 6 ka or 127 ka) to illustrate
138 the calendar effect will inevitably be confounded by the climatic response to changes in insolation (and other boundary
139 conditions). The impact on the analysis of paleoclimatic simulations of the calendar effect can alternatively be assessed by
140 assuming that the long-term mean difference in climate (also referred to as the experiment minus control “anomaly”) is zero
141 everywhere, illustrating the “pure” calendar effect. Pseudo-daily interpolated values (or actual daily output, if available) of
142 present-day monthly data can then simply be reaggreated using an appropriate paleo calendar and compared with the present-
143 day data. (The pseudo-daily values used here were obtained by interpolating monthly data to a daily time-step using the
144 monthly mean-preserving algorithm described below.)

145 The “pure” calendar effect is demonstrated here using present-day monthly long-term mean (1981-2010) values of near-surface
146 air temperature (*tas*) from the Climate Forecast System Reanalysis (CFSR; Saha et al., 2010;
147 <https://esgf.nccs.nasa.gov/projects/ana4mips/>), and monthly precipitation rate (*precip*) from the CPC Merged Analysis of
148 Precipitation (CMAP; Xie and Arkin, 1997; <https://www.esrl.noaa.gov/psd/data/gridded/data.cmap.html>) (Fig. 10). (These
149 data were chosen because they are global in extent and are of reasonably high spatial resolution.) If it is assumed that there is
150 no long-term mean difference between a present-day and paleo simulation (by adopting the present-day data as the simulated
151 paleo data), then the unadjusted present-day data can be compared with present-day data adjusted to the appropriate paleo
152 month lengths. The calendar-adjusted minus unadjusted differences will therefore reveal the inverse of the built-in calendar
153 effect “signal” in the unadjusted data, that might readily be interpreted in terms of some specific paleoclimatic mechanisms,



154 while being instead a data analytical artefact. Positive values on the maps (Figs. 11-13) indicate, for example, where
155 temperatures would be higher or precipitation greater if a fixed-angular calendar were used to summarize the paleo data.

156 3.1 Monthly temperature

157 The impacts of using the appropriate calendar to summarize the data (as opposed to not) are large, often exceeding 1 °C in
158 absolute value (Fig. 11). The effects are spatially variable, and are not simple functions of latitude as might be initially
159 expected, because the effect increases with the amplitude of the annual cycle (which has a substantial longitudinal component)
160 for temperature regimes that are in phase with the annual cycle of insolation. For temperature regimes that are out of phase
161 with insolation, the calendar-adjusted minus unadjusted values would be negative, and largest when the temperature variations
162 were exactly out of phase. (If there were no annual cycle, i.e. if a climate variable remained constant over the course of a year,
163 the calendar effect would be zero.) The interaction between the annual cycle and the direct calendar effect on insolation
164 produces patterns of the overall calendar effect that happen to resemble some of the large-scale responses that are frequently
165 found in climate simulations, both past and future, such as high-latitude amplification or damping, continental-ocean contrasts,
166 interhemispheric contrasts and changes in seasonality of temperature (cf. Izumi et al., 2013). Because the month-length
167 calculations use the Northern Hemisphere vernal equinox as a fixed origin for the location of Earth along its orbit, the effects
168 seem to be small during the months surrounding the equinox (i.e. February through April, Fig. 11), and indeed the selection of
169 a different origin would produce different apparent effects (see Jousaumme and Braconnot, 1997, Sect. 2.1). However, the
170 selection of a different origin would not change the relative (to present) length of time it would take Earth to transit any
171 particular angular segment of its orbit.

172 At 6 ka, the largest calendar effects on temperature can be observed over the Northern Hemisphere continents for the months
173 from September through December (Fig. 11), consistent with the earlier beginning of these months (Fig. 2) and the direct
174 calendar effect on insolation at 45° N (Fig. 3). For example, in the interior of the northern continents, as well as North Africa,
175 temperature is in phase with insolation, and so the calendar effect on insolation (Fig. 3), which produces strongly positive
176 differences from August through November, is reflected by the calendar effect on temperature. Over the northern oceans,
177 temperature is broadly in phase with insolation, but with a lag, which reduces the magnitude of the effect and gives rise to an
178 apparent land-ocean contrast that otherwise might be interpreted in terms of some particular paleoclimatic mechanism. The
179 calendar effect on temperature from January through March produces negative calendar-adjusted minus unadjusted values in
180 the northern continental interiors (Fig. 11), which is also consistent with the calendar effect on insolation. In the Southern
181 Hemisphere at 6 ka, the calendar effects on temperature produce generally negative differences, which is consistent with the
182 calendar effects on mid-month insolation at 45° S (Fig. 5), which produce generally negative differences throughout the year,
183 particularly during the months of August through November. Like the continent – ocean contrast in the Northern Hemisphere,
184 the Northern Hemisphere – Southern Hemisphere contrast in the calendar effect on temperature also could be interpreted in
185 terms of one or another of the mechanisms thought to be responsible for interhemispheric temperature contrasts.



186 At 127 ka, the calendar effect on temperature is broadly similar to that at 6 ka over the months from September through March,
187 but differs in sign from April through July, and in magnitude in August (Fig. 11). These patterns are also consistent with the
188 direct calendar effects on insolation. At 127 ka, the calendar effect on insolation produces strongly positive differences in the
189 Northern Hemisphere earlier in the northern summer than at 6 ka (Fig. 3), while at 45° S the calendar effect on insolation
190 produces strongly negative differences in July and persists that way through November (Fig. 5). At 116 ka, perihelion occurs
191 in late December, in comparison to late June at 127 ka (Figs. 1 and 6), and not surprisingly the calendar effect on temperature
192 is nearly the inverse of that at 127 ka (Fig. 11). This pattern has important implications for paleoclimatic studies, because in
193 addition to all of the changes in the forcing and the paleoclimatic responses accompanying the transition out of the last
194 interglacial, the possibility that some of the apparent simulated changes between 127 and 116 ka may be an artefact of data-
195 analysis procedures cannot be discounted.

196 At 97 ka, a time selected to illustrate a different orbital configuration (i.e. one with boreal spring months occurring closer to
197 the June solstice) than the similar (6 ka and 127 ka) or contrasting (127 and 116 ka) configurations, the calendar effect on
198 temperature in the Northern Hemisphere (Fig. 11) shows a switch from positive differences in the early boreal summer (May
199 and June) to negative in the late summer (August and September). This switch is again consistent with the direct calendar
200 effect on insolation (Fig. 3). Like the other times, the spatial variations in the calendar effect could easily be interpreted in
201 terms of one kind of paleoclimatic mechanism or another.

202 **3.2 Mean temperature of the warmest and coldest months**

203 Although the calendar effects on monthly mean temperature show some sub-continental scale variability, the overall patterns
204 are of relatively large spatial scales, and are interpretable in terms of the direct orbital effects on month lengths and insolation.
205 The calendar effects on the mean temperature of the warmest (MTWA) and coldest (MTCO) calendar months (and their
206 differences) are much more spatially variable (Fig. 12). This variability arises in large part because of the way these variables
207 are usually defined (e.g. as the mean temperature of the warmest or coldest conventionally defined month, as opposed to the
208 temperature of the warmest or coldest 30-day interval), but also because the calendar adjustment can result in a change in the
209 specific month that is warmest or coldest. These effects are compounded when calculating seasonality (as MTWA minus
210 MTCO). Other definitions of the warmest and coldest month are possible, such as the warmest consecutive 30-day period
211 during the year (e.g. Caley et al., 2014), and such definitions will not be susceptible to the calendar effect. In practice, however,
212 paleoclimatic reconstructions based on calibrations or forward-model simulations routinely use conventional calendar-month
213 definitions of the warmest and coldest months and of seasonality (Bartlein et al., 2011; Harrison et al., 2014), and often only
214 monthly output from paleoclimatic simulations is available necessitating consistent definitions when summarizing model
215 output.



216 In the particular set of example times chosen here, the magnitudes of the calendar effects are also smaller than those of
217 individual months because, as it happens, the calendar effects in January and February (typically coldest months in the Northern
218 Hemisphere) and July and August (typically warmest months in the Northern Hemisphere) are not large. There are also some
219 surprising patterns. The inverse relationship between the calendar effects at 116 ka and 127 ka that might be expected from
220 inspection of the monthly effects (Fig. 11) are not present, while the calendar effects on MTCO and MTWA at 97 ka and 116
221 ka tend to resemble one another. Across the four example times, there is an indistinct, but still noticeable pattern in reduced
222 seasonality (MTWA minus MTCO) between the adjusted and unadjusted values, which like the other patterns described above
223 could tempt interpretation in terms of some specific climatic mechanisms.

224 3.3 Monthly precipitation

225 In contrast to the large spatial-scale patterns of the calendar effect on temperature, the patterns of the calendar effect on
226 precipitation rate are much more complex, showing both continental-scale patterns (like those for temperature), but also
227 smaller-scale patterns that are apparently related to precipitation associated with the ITCZ and regional and global monsoons
228 (Fig. 13). The continental-scale patterns are evident in the calendar effects at 6 and 127 ka, particularly in the months from
229 September through November (Fig. 13), where it also can be noted (especially over the mid-latitude continents in both
230 hemispheres) that there is a positive association with the calendar effect on temperature. This association is related simply to
231 similarities in the shapes of the annual cycles of those variables, and not to some kind of more elaborate thermodynamic
232 constraint. At 116 ka, as for temperature, the large-scale calendar-effect patterns appear to be nearly the inverse of those at
233 127 ka. The smaller-scale kind of pattern is well illustrated at 127 ka in the tropical North Atlantic, sub-Saharan Africa and
234 south Asia. There, negative calendar-adjusted minus unadjusted values can be noted for June through August, giving way to
235 positive differences from September through November, and the same transition appears inversely at 116 ka. Another example
236 can be found in the South Pacific Convergence Zone in austral spring and early summer (September through November) at 6
237 and 127 ka, where generally positive differences between calendar-adjusted and unadjusted values in July and August gives
238 way to negative differences from September through December. This second kind of pattern, most evident in the subtropics,
239 is not mirrored by the calendar effects on temperature.

240 Overall, the magnitude and spatial patterns of the calendar effects on temperature and precipitation (Figs. 11 and 13) resemble
241 those in the paleoclimatic simulations and observations that we attempt to explain in mechanistic terms. Depending on the
242 sign of the effect, neglecting to account for the calendar effects could spuriously amplify some “signals” in long-term mean
243 differences between experiment and control simulations, while damping others.

244 3.4 Calendar effects and transient experiments

245 Calendar effects must also be considered in the analysis of transient climate-model simulations (even if those data are available
246 on the daily time step). This can be illustrated for a variety of variables and regions using data from the TraCE-21k transient



247 simulations (Liu et al., 2009; <https://www.earthsystemgrid.org/project/trace.html>). The series plotted in Fig. 14 are area-
248 averages for individual months on a yearly time step, with 100-yr (window half-width) locally weighted regression curves
249 added to emphasize century-timescale variations. The original yearly time-step data were aggregated using a perpetual “no
250 leap” (365-day) calendar (using the present-day month lengths for all years). The gray and black curves on Fig. 14 show these
251 unadjusted “original” values, while the colored curves show month-length adjusted values (i.e. pseudo-daily interpolated
252 values, reaggregated using the appropriate paleo fixed-angular calendar). Area averages were calculated for ice-free land
253 points.

254 Figure 14a shows area-weighted averages for 2 m air temperature for a region that spans 15 to 75° N and -170 to 60° E, the
255 region used by Marsicek et al. (2018) to discuss Holocene temperature trends in simulations and reconstructions. The largest
256 differences between month-length adjusted values and unadjusted values occur in October between 14 and 6 ka, when
257 perihelion occurred during the northern summer months. October month lengths during this interval were generally within
258 one day of those at present (Fig. 1), but the generally shorter months from April through September resulted in Octobers
259 beginning up to ten days earlier in the calendar than at present, i.e. closer in time to the boreal summer solstice (Fig. 2). The
260 calendar-effect adjusted October values therefore average up to 4 °C higher than the unadjusted values during this interval
261 (Fig. 14a), consistent with the direct calendar effects on insolation at 45° N (Fig. 3). The calendar effect also changes the
262 shape of the temporal trends in the data, particularly during the Holocene. October temperatures in the unadjusted data showed
263 a generally increasing trend over the Holocene (i.e. since 11.7 ka), reaching a maximum around 3 ka, comparable with present-
264 day values, while the adjusted data reached levels consistently above present-day values by 7.5 ka. The unadjusted October
265 temperature data could be described as reaching a “Holocene thermal maximum” only in the late Holocene (i.e., after 4 ka),
266 while the adjusted data display more of a mid-Holocene maximum. As is the case with the mapped assessments of the “pure”
267 calendar effect, the differences between unadjusted and adjusted time series are of the kind that could be interpreted in terms
268 of various hypothetical mechanisms. For example, the calendar-effect adjustment advances the time of occurrence of a
269 Holocene thermal maximum in October by about 3 kyr for North America and Europe.

270 As in North America and Europe, the adjusted temperature trends in Australia (10 to 50° S and 110 to 160° E) (Fig. 14b) are
271 consistent with the direct calendar effects on insolation (i.e. for 45° S, Fig. 5). The difference between adjusted and unadjusted
272 values are again largest in October between 14 and 6 ka, but the difference is the inverse of that for the North America and
273 Europe region, because the annual cycle of temperature for Australia is inversely related to the annual cycle of the insolation
274 anomalies (Fig. 9) and so to the direct calendar effects on insolation (Fig. 5). Again, the shapes of the Holocene trends in the
275 adjusted and unadjusted data are noticeably different. In the Australia (Fig. 14b) and North America and Europe (Fig. 14a)
276 examples, relatively large areas are being averaged, and the calendar effect becomes more apparent as the size of the area
277 decreases. Notably, the effect does not completely disappear at the largest scales, i.e. for area-weighted averages for the globe
278 (for ice-free land grid cells) (Fig. 14c). The differences are smaller, but still discernible.



279 In the Northern Hemisphere (African-Asian) Monsoon region (0 to 30° N and -30 to 120° E), the calendar effects on
280 precipitation rate are similar to those on temperature in the mid-latitudes because the annual cycle of precipitation is roughly
281 in phase with that of insolation (Fig. 7). There is little effect in the winter and spring, but a substantial effect in summer and
282 autumn over the interval from 17 ka to about 3 ka (Fig. 14d). The calendar effect reverses sign between July and August
283 (when the month-length adjusted precipitation rate values are less than the unadjusted ones) and September and October (when
284 the adjusted values are greater than the unadjusted ones). In July, the timing of relative maxima and minima in the two data
285 sets is similar, while in October, in particular, the Holocene precipitation maximum is several thousand years earlier in the
286 adjusted data than in the unadjusted.

287 The time-series expression of the latitudinally reversing calendar effect on precipitation rate evident in Fig. 13 (e.g. July vs.
288 October at 127 ka) can be illustrated by comparing precipitation or precipitation minus evaporation ($P - E$) for the North
289 African (sub-Saharan) Monsoon region (5 to 17° N and -5 to 30° E) with the Mediterranean region (31 to 43° N and -5 to 30°
290 E) (Fig. 14e and 14f). The differences between the adjusted and unadjusted data in the North African region (Fig. 14e) parallel
291 that of the larger monsoon region (Fig. 14d). The Mediterranean region, which is characteristically moister in winter and drier
292 in summer shows the reverse pattern: when the calendar-adjusted minus unadjusted $P - E$ difference is positive in the monsoon
293 region, it is negative in the Mediterranean region. Dipoles are frequently observed in climatic data, both present-day and paleo,
294 and are usually interpreted in terms of broad-scale circulation changes in the atmosphere or ocean. This example illustrates
295 that they could also be artefacts of the calendar effect. Such changes in timing of extrema also could influence the interpretation
296 of phase relationships among simulated time series and time series of potential forcing (Joussaume and Braconnot, 1997; Timm
297 et al., 2008; Chen et al., 2011). The impacts of the calendar effect on temporal trends in transient simulations (Fig. 14), when
298 compounded by the spatial effects (Figs. 11-13), make it even more likely spurious climatic mechanisms could be inferred in
299 analyzing transient simulations than in the simpler time-slice simulations.

300 **4 PaleoCalAdjust v 1.0**

301 The approach we describe here for adjusting model output reported either as monthly data (using fixed-length definitions of
302 months) or as daily data to reflect the calendar effect (i.e. to make month-length adjustments) has two fundamental steps: 1)
303 pseudo-daily interpolation of the monthly data on a fixed-month-length calendar (which, when actual daily data are available,
304 is not necessary), followed by 2) aggregation of those daily data to fixed-angular months defined for the particular time of the
305 simulations. The second step obviously requires the calculation of the beginning and ending days of each month as they vary
306 over (“geological”) time, which in turn depends on the orbital parameters. The definition of the beginning and ending days of
307 a month in a “leap-year,” “Gregorian,” or “proleptic Gregorian” calendar (<http://cfconventions.org>) additionally depends on
308 the timing of the (northern) vernal equinox, which varies from year to year. Here we describe the pseudo-daily interpolation
309 method first, followed by a discussion of the month-length calculations. Then we describe the calendar-adjustment program,



310 along with a few demonstration programs that exercise some of the individual procedures. All of the programs, written in
311 Fortran 90, are available (see *Code and data availability* section).

312 4.1 Pseudo-daily interpolation

313 The first step in adjusting monthly time-step model output to reflect the calendar effect is to interpolate the monthly data (either
314 long-term means or time-series data) to pseudo-daily values. (A step that is not required if the data are daily time-step values.)
315 It turns out that the most common way of producing pseudo-daily values, linear interpolation between monthly means, is not
316 mean preserving; the monthly (or annual) means of the interpolated daily values will generally not match the original monthly
317 values. An alternative approach, and the one we use here, is the mean-preserving “harmonic” interpolation method of Epstein
318 (1991), which is easy to implement, and performs the same function as the parabolic-spline interpolation method of Pollard
319 and Reusch (2002).

320 The linear and mean-preserving interpolation methods can be compared using the Climate Forecast System Reanalysis (CFSR)
321 near-surface air temperature and CPC Merged Analysis of Precipitation (CMAP) 1981-2010 long-term mean data (Fig. 15).
322 A typical example for temperature appears in Fig. 15a, for a gridpoint near Madison, Wisconsin (USA). The difference
323 between the annual mean values of the interpolated data for the two approaches is small and similar (ca. 2.0×10^{-6}), but the
324 difference between the original monthly means and the monthly mean of the linearly interpolated daily values can exceed 0.8
325 °C in some months (e.g. December). (The differences from the original monthly means for the mean-preserving interpolation
326 method are less than 1.0×10^{-3} °C for every month in Fig. 15a.) Fig. 15b shows an example for a grid point in Australia, where
327 again the difference between the original monthly means and the monthly means of the linearly interpolated daily values is not
328 negligible (i.e. 0.4 °C). Similar results hold for precipitation (Fig. 15c), where the difference can exceed 0.1 mm d⁻¹). Like
329 other harmonic-based approaches, the Epstein approach can create interpolated curves that are wavy (see Pollard and Reusch
330 (2002) for discussion), but these effects are small enough to not be practically important in nearly all cases. The pathological
331 case for precipitation is shown in Fig. 15d, at a grid point in the Indian Ocean. Here, the difference between an original
332 monthly mean value and one calculated using the mean-preserving interpolation method reaches -0.12 mm d⁻¹ in March and
333 April, but the differences between the original monthly means and the monthly means of the linearly interpolated daily values
334 are nearly three times larger.

335 The map patterns of the interpolation errors (the monthly mean values recalculated using the pseudo-daily interpolated values
336 minus the original values) appear in Fig. 16. (Note the differing scales for the linear-interpolation errors and the mean-
337 preserving-interpolation errors.) The linear interpolation errors are quite large, with absolute values exceeding 1 °C and 1 mm
338 d⁻¹, and have distinct seasonal and spatial patterns: underpredictions of Northern Hemisphere temperature in summer (and
339 overpredictions in winter), and underpredictions of precipitation in the wet season (e.g. southern Asia in July) and
340 overpredictions in the dry season (southern Asia in May). The magnitude and patterns of these effects again rival those we



341 attempt to infer or interpret in the paleo record. The mean-preserving interpolation errors for temperature are very small, and
342 show only vague spatial patterns (note the differing scales). The errors for precipitation are also quite small, but can be locally
343 larger, as in the pathological case illustrated above. However, the map patterns of the interpolation errors strongly suggest that
344 those cases are not practically important.

345 The mean-preserving interpolation method is implemented in the Fortran 90 module named `pseudo_daily_interp_subs.f90`.
346 The subroutine `hdaily(...)` manages the interpolation, first getting the harmonic coefficients (Eq. 6 of Epstein, 1991) using the
347 subroutine named `harmonic_coeffs(...)` and then applying these coefficients in the subroutine `xthat(...)` to get the interpolated
348 values.

349 4.2 Month-length calculations

350 Calculation of the length and the beginning, middle and ending (real-number or fractional) days of each month at a particular
351 time is based on the algorithm described by Kutzbach and Gallimore (1988, see also Kutzbach and Otto-Bliesner, 1982). The
352 algorithm allows the calculation of the length of time, in real-number or fractional days, for the Earth to traverse an angular
353 portion of its orbit, i.e. it provides the length of months or seasons in a fixed-angular calendar for any particular time. By
354 choosing a fixed reference day (i.e. the vernal equinox), the beginning, middle, and ending days of months can be calculated.
355 Application of this algorithm requires as input eccentricity and the longitude of perihelion (in degrees) relative to the vernal
356 equinox, and the generalization of the approach to other calendars, such as the “proleptic Gregorian” calendar (that includes
357 leap years, <http://cfconventions.org>), also requires the (real-number or fractional) day of the vernal equinox. To calculate the
358 orbital parameters using the Berger (1978) solution, and the timing of the (northern) vernal equinox (as well as insolation
359 itself), we adapted a set of programs provided by National Aeronautics and Space Administration, Goddard Institute for Space
360 Studies (<https://data.giss.nasa.gov/ar5/solar.html>).

361 The approach adopted by Kutzbach and Gallimore (1988) is based on an approximation that describes the rate of change in
362 celestial longitude, ϕ , with time (over the year):

$$363 \quad dt/d\phi = 1 + 2e \sin((2\pi/360)(\phi - \phi_p)) \quad (1)$$

364 which depends on eccentricity, e , and the date of perihelion, expressed as a phase angle, ϕ_p , defined so that $\sin((2\pi/360)(\phi -$
365 $\phi_p)) = -1$ at the celestial longitude of perihelion, and where ϕ , and ϕ_p are expressed in units of degrees and t in days (their
366 equation A1). After ϕ_p has been determined, the amount of time (in real-number or fractional days) required to traverse a given
367 number of degrees of celestial longitude from the vernal equinox can be determined by an integration of A1 (their equation
368 A2):

$$369 \quad t = \phi - 2e (\cos((2\pi/360)(\phi - \phi_p)) - \cos((2\pi/360)\phi))(360/2\pi) \quad (2)$$

370 We implemented this approach in the subroutine `kg_monlen_360(...)` in the Fortran 90 module named `month_length_subs.f90`.
371 (This subroutine is not actually used in practice because it can handle only 360-day year calendars, but it illustrates the basic



372 ideas of the approach.) After initializing a set of day numbers and angular differences from the vernal equinox (assumed to
373 be fixed at 80 days after the beginning of the year) (Step 1 in `kg_monlen_360(...)`), we determine ϕ_p by advancing along the
374 orbit at 0.001-day increments from the vernal equinox, and selecting ϕ_p as the value that minimizes $-1 - \sin((2\pi/360)(\phi - \phi_p))$
375 (Step 2). Then the traverse time since the vernal equinox is calculated for each day using Kutzbach and Gallimore's (1988)
376 equation A2 (Step 3), and this traverse time is used to get the relative length of each day through simple differencing (Step 4).
377 Finally, the length of each month (in real-number or fractional days) is determined by accumulation (Step 5).

378 4.3 Simulation ages and simulation years

379 Inspection shows that different climate models employ different starting dates in their output files for both present-day
380 (*piControl*) and paleo (e.g. *midHolocene*) simulations (<https://esgf-node.llnl.gov/projects/cmip5/>). For models that use a
381 noleap (constant 365-day year) calendar, such as CCSM4 (Otto-Bliesner, 2014), the starting date is not an issue, but for MPI-
382 ESM-P (Jungclaus et al., 2012), which uses a proleptic Gregorian calendar, or CNRM-CM5 (Sénési et al., 2014), with a
383 “standard” (i.e. mixed Julian/Gregorian) calendar as examples, the specific starting date influences the date of the vernal
384 equinox through the occurrence of individual leap years. For example, in the CMIP5/PMIP4 *midHolocene* simulations, output
385 from MPI-ESM-P starts in 1850 CE, and that from CNRM-CM5 in 2050 CE (and it can be verified that leap years in those
386 output files occur in a fashion consistent with the “modern” calendar). Consequently, we need to make a distinction between
387 two notions of time here: 1) the simulation age, expressed in (negative) years BP (i.e. before 1950 CE), and 2) the simulation
388 year, expressed in years CE. The simulation age controls the orbital parameter values, while the simulation year, along with
389 the specification of the CF-compliant calendar attribute (<http://cfconventions.org>), controls the date and time of the vernal
390 equinox.

391 4.4 Month-length programs and subprograms

392 Month lengths are calculated in the subroutine, `get_month_lengths(...)` (contained in the Fortran 90 module named
393 `month_length_subs.f90`), that in turn calls the subroutine `kg_monlen(...)` to get real-type month lengths for a particular
394 simulation age and year. (The subroutine `get_month_lengths(...)` can be exercised to produce tables of month lengths,
395 beginning, middle and ending days of the kind used to produce Figs. 1-5 and 7-9 using a driver program named
396 `month_length.f90`.) The subroutine `get_month_lengths(...)` uses two other modules, `GISS_orbpar_subs.f90` and
397 `GISS_srevents_subs.f90` (based on programs downloaded from GISS (<https://data.giss.nasa.gov/ar5/solar.html>)), to get the
398 orbital parameters and vernal equinox dates.

399

400 The specific tasks involved in the calculation of either a single year's set of month lengths, or a series of month lengths for
401 multiple years, include the following steps, implemented in `get_month_lengths(...)`:

402 1. generate a set of “target” dates based on the simulation ages and simulation years;



- 403 2. obtain the orbital parameters for 0 ka (1950 CE), which will be used to adjust the calculated month-length values to
404 the conventional definition of months for 1950 CE as the reference year;
- 405 3. obtain the present-day (i.e. 1950 CE) month lengths for the appropriate calendar.
- 406 Then loop over the simulation ages and simulation years, and for each combination:
- 407 4. obtain the orbital parameters for each simulation age, using the subroutine `GISS_orbparams(...)`;
- 408 5. calculate real-type month lengths for the appropriate calendar using `kg_monlen(...)`;
- 409 6. adjust (using the subroutine `adjust_to_reference(...)`) those month length values to the reference year (e.g. 1950
410 CE) and its conventional set of month-length definitions so that, for example, January will have 31 days, February 28
411 or 29 days, etc., in that reference year;
- 412 7. further adjust the month-length values to ensure that the individual monthly values will sum exactly to the year length
413 in days using `adjust_to_yeartot(...)`;
- 414 8. convert real-type month lengths to integers using `integer_monlen(...)` (These integer values are not used anywhere,
415 but may be useful in conceptualizing the pattern of month-length variations over time.);
- 416 9. determine the mid-March day, using `GISS_srevents(...)` to get the vernal equinox date for calendars in which it varies;
417 and
- 418 10. calculate real- and integer-type beginning, middle and ending days using `imon_midbegend(...)` and `rmon_midbegend(...)`
419 for integer- and real-number definitions of the months.

420 **4.5 Month-length tables and time series**

421 Tables and time series of month lengths, beginning, middle and ending days, and dates of the vernal equinox can be calculated
422 using the program `month_length.f90`. This program reads an “info file” (`month_length_info.csv`) consisting of an identifying
423 output file name prefix, the calendar type, the beginning and ending simulation age (in years BP), and the age step, and the
424 beginning simulation year (in years CE) and the number of simulation years. Note that in the approach described above, orbital
425 parameters are calculated once per year (step 4 in Sect. 4.4), and are assumed to apply for the whole year. This assumption
426 can lead to small differences (ranging from -0.000863 to 0.000787 days over the past 22 kyr with a mean of -0.0000389 days)
427 in the ending day of one year and the beginning day of the next.

428 **5 Paleo calendar adjustment**

429 The objective of the principal calendar-adjustment program `cal_adjust_PMIP3.f90` is to read and clone a “CMIP5/PMIP3”-
430 formatted netCDF file, replacing the original monthly or daily data with calendar-adjusted data, i.e. data aggregated using a
431 fixed-angular calendar appropriate for a particular paleo experiment. In the case of monthly input data, either climatological
432 long-term means or monthly time-series, the data are first interpolated to a daily time step, and then reaggregated to monthly
433 time-step mean values using an appropriate paleo calendar. In the case of daily input data, the interpolation step is obviously



434 unneeded, and so the data are simply aggregated to the monthly time step. In both cases, new time-coordinate variables are
435 created (consistent with the paleo calendar), and all other dimension information, coordinate variables and global attributes
436 are copied, and augmented by other attribute data that indicate that the data have been adjusted. The reading and rewriting of
437 the netCDF file is handled by subroutines in a module named `CMIP5_netCDF_subs.f90` and various modules and subprograms
438 for month-length calculations described above are also used here.

439

440 **5.1 Interpolation and (re)aggregation**

441 The pseudo-daily interpolation and (re)aggregation is done using two subroutines `mon_to_day_ts(...)` and `day_to_mon_ts(...)`
442 in the module `calendar_effects_subs.f90`. The pseudo-daily interpolation is done a year at a time, creating slight
443 discontinuities between one year and the next in the case of transient or multi-year “snapshot” simulations. The subroutine
444 `mon_to_day_ts(...)` has options for smoothing those discontinuities, and restoring the long-term mean of the interpolated daily
445 data to that of the original monthly data.

446 The (re)aggregation of the daily data is also done a year at a time by collecting the daily data for a particular year, and “padding”
447 it at the beginning and end with data from the previous and following year if available, as in transient or multi-year simulations
448 (to accommodate the fact that under some orbital configurations the first day of the current year may occur in the previous
449 year, or the last day in the following year; Fig. 1). For example, at 6 ka, the changes in the shape of the orbit and the
450 consequently longer months from January through March (32.5, 29.5 and 32.4 days, respectively) displaces the beginning of
451 January four days into the previous year, with the last day of December consequently falling just before day 361 in a 365-day
452 year. In the case of long-term mean “climatological” data (“Aclim” data), the padding is done with ending and beginning days
453 of the single year of pseudo-daily data.

454 The calculation of monthly means is done by calculating weighted averages of the days that overlap with a particular month
455 as defined by the (real-number or fractional) beginning and ending days of that month (from the subroutine
456 `get_month_lengths(...)`). Each whole day in that interval gets a weight of 1.0, and each partial day gets a weight proportional
457 to its part of a whole day. It should be noted that in transient simulations, annual averages, constructed either by averaging
458 actual or pseudo-daily data (or by month-length weighted averages) will differ from the unadjusted data.

459 **5.2 Processing individual netCDF files**

460 At present, the program reads an “info file” that provides file and variable details, and this info file will be easily modified to
461 accommodate “CMIP6/PMIP4” formatted files (<https://pcmdi.llnl.gov/CMIP6/Guide/modelers.html#5-model-output-requirements>) as they become available. The fields in the info file include (for each netCDF file), the variable (e.g. “tas”,
462 “pr”), the “realm-plus-time-frequency” type (e.g. “Amon”, “Aclim”, ...), the model name, the experiment name (e.g.
463 “midHolocene”), the ensemble member (e.g. “r1i1p1”), and the simulation year beginning date and ending date (as a



465 YYYYMM or YYYYMMDD string). An input filename “suffix” field is also read (which is usually blank, but is “-clim” for
466 Aclim-type files), as is an output filename “suffix” field (e.g. “_cal_adj”), which is added to the output filename to indicate
467 that it has been modified from the original. The info file also contains the simulation age beginning and end (in years BP), the
468 increment between simulation ages (usually 1 in the application here), the beginning simulation year (years CE) and the number
469 of simulation years. This information could also be gotten by parsing the netCDF file name and reading the calendar attribute
470 and time-coordinate variables, but that would add to the complexity of the program.

471 The output netCDF files have the string “_cal_adj” appended to the end of the filename. In the case of monthly time series
472 (e.g. “Amon”) or long-term means (e.g. “Aclim”) the file names are otherwise the same as the input data. In the case of the
473 daily input data, with “day” as the “realm plus time frequency” string, that string is changed to “Amon2”.

474 The adjustment of a file using `cal_adjust_PMIP3.f90` includes the following steps:

475

- 476 1. read the info file, construct various file names, allocate month-length variables;
- 477 2. generate month lengths using the subroutine `get_month_lengths(...)`;
- 478 3. open input and output netCDF files; and for each file
- 479 4. redefine the time-coordinate variable as appropriate using the subroutines `new_time_day(...)` and `new_time_month(...)`
480 in the module `CMIP5_netCDF_subs.f90`;
- 481 5. create the new netCDF file, copy the dimension and global attributes from the input file using the subroutine
482 `copy_dims_and_glatts(...)`, define the output variable using the subroutine `define_outvar(...)`;
- 483 6. get the input variable to be adjusted;
- 484 7. for each model grid point, get calendar-adjusted values as described above using the subroutines `mon_to_day_ts(...)`
485 and `day_to_mon_ts(...)`; and
- 486 8. write out the adjusted data, and close the output file.

487 5.3 Further examples

488 Five other main programs that serve as “drivers” for some of the subroutines or that demonstrate particular aspects of
489 procedures used here are included in the GitHub repository for the programs (<https://github.com/pjbartlein/PaleoCalAdjust>):

- 490 ▪ `GISS_orbpar_driver.f90` and `GISS_srevents_driver.f90`; Main programs that call the subroutines
491 `GISS_orbpars(...)` and `GISS_srevents(...)` to produce tables of orbital parameters and “solar events” like the dates of
492 equinoxes, solstices and perihelion and aphelion.
- 493 ▪ `demo_01_pseudo_daily_interp.f90`; Main program that demonstrates linear and mean-preserving pseudo-daily
494 interpolation.
- 495 ▪ `demo_02_adjust_1yr.f90`; Main program that demonstrates the paleo calendar adjustment of a single year’s data.



- 496 ▪ demo_03_adjust_TraCE_ts.f90; Main program that demonstrates the adjustment of a 22040 year-long time series of
497 monthly TraCE-21k data.

498 **6 Summary**

499 As has been done previously (e.g. Kutzbach and Otto-Bliesner, 1982; Kutzbach and Gallimore, 1988; Jousaumme and
500 Braconnot, 1997; Pollard and Reusch, 2002; Timm et al., 2008; Chen et al., 2011; Kageyama et al., 2018), we have described
501 the substantial impacts of the paleo calendar effect on the analysis of climate-model simulations, and provide what we hope is
502 a straightforward way of making adjustments that incorporate the effect. The interval between previous calls to include
503 consideration of the calendar effect in paleoclimate analyses has ranged between three and nine years over the past nearly four
504 decades, with a median interval of six years. The size and impact of the calendar effect warrant its consideration in the analysis
505 of paleo simulations, and we hope that by providing a relatively easy-to-implement method, that will become the case.

506 **Code and data availability**

507 The Fortran 90 source code (main programs and modules), example data sets, and the data used to construct the figures are
508 available from Zenodo (<https://zenodo.org/>) at the following URL: <https://doi.org/10.5281/zenodo.1478824> and .from GitHub
509 (<https://github.com/pjbartlein/PaleoCalAdjust>). All climate data used here are available for download at the URLs cited in the
510 text.

511 **Author contribution**

512 PB designed the study, developed the Fortran 90 programs, and wrote the first draft of the manuscript. Both authors contributed
513 to the final version of the text.

514 **Competing Interests**

515 The authors declare that they have no conflict of interest.

516

517 **Acknowledgements:** We thank Jay Alder, Martin Claussen, and Anne Dallmeyer for their comments on earlier versions of
518 the text. This publication is a contribution to PMIP4. TraCE-21ka was made possible by the DOE INCITE computing
519 program, and supported by NCAR, the NSF P2C2 program, and the DOE Abrupt Change and EaSM programs. CMAP
520 precipitation data were provided by the NOAA/OAR/ESRL PSD, Boulder, Colorado, USA, from their Web site at
521 <https://www.esrl.noaa.gov/psd/>. CFSR near-surface air-temperature data were obtained from
522 <https://esgf.nccs.nasa.gov/projects/ana4mips/> (for the original source see <http://cfs.ncep.noaa.gov>). Maps were prepared using



523 NCL, the NCAR Command Language (Version 6.4.0 [Software], 2017, Boulder, Colorado: UCAR/NCAR/CISL/TDD.
524 <http://dx.doi.org/10.5065/D6WD3XH5>). S.S. was supported by the U.S. Geological Survey Land Change Science Program.
525 Any use of trade, firm, or product names is for descriptive purposes only and does not imply endorsement by the U.S.
526 Government.

527 References

528 Bartlein, P. J., Harrison, S. P., Brewer, S., Connor, S., Davis, B. A. S., Gajewski, K., Guiot, J., Harrison-Prentice, T. I.,
529 Henderson, A., Peyron, O., Prentice, I. C., Scholze, M., Seppa, H., Shuman, B., Sugita, S., Thompson, R. S., Viau, A. E.,
530 Williams, J., and Wu, H.: Pollen-based continental climate reconstructions at 6 and 21 ka: a global synthesis, *Climate*
531 *Dynamics*, 37, 775-802, <https://doi.org/10.1007/s00382-010-0904-1>, 2011.

532

533 Berger, A. L.: Long-term variations of daily insolation and Quaternary climatic changes, *J. Atmos. Sci.*, 35, 2362-2367,
534 [https://doi.org/10.1175/1520-0469\(1978\)035<2362:LTVODI>2.0.CO;2](https://doi.org/10.1175/1520-0469(1978)035<2362:LTVODI>2.0.CO;2), 1978.

535

536 Caley, T., Roche, D. M., and Renssen, H.: Orbital Asian summer monsoon dynamics revealed using an isotope-enabled global
537 climate model, *Nature Communications*, 5, 5371, <https://doi.org/10.1038/ncomms6371>, 2014.

538

539 Chen, G.-S., Kutzbach, J. E., Gallimore, R., and Liu, Z.: Calendar effect on phase study in paleoclimate transient simulation
540 with orbital forcing, *Clim. Dynam.*, 37, 1949-1960, <https://doi.org/10.1007/s00382-010-0944-6>, 2011.

541

542 Epstein, E. S.: On obtaining daily climatological values from monthly means, *J. Climate*, 4, 365-368,
543 [https://doi.org/10.1175/1520-0442\(1991\)004<0365:OODCVF>2.0.CO;2](https://doi.org/10.1175/1520-0442(1991)004<0365:OODCVF>2.0.CO;2), 1991.

544

545 Harrison, S. P., Bartlein, P. J., Brewer, S., Prentice, I. C., Boyd, M., Hessler, I., Holmgren, K., Izumi, K., and Willis, K.:
546 Climate model benchmarking with glacial and mid-Holocene climates, *Climate Dynamics*, 43, 671-688,
547 <https://doi.org/10.1007/s00382-013-1922-6>, 2014.

548

549 Ivanovic, R. F., Gregoire, L. J., Kageyama, M., Roche, D. M., Valdes, P. J., Burke, A., Drummond, R., Peltier, W. R., and
550 Tarasov, L.: Transient climate simulations of the deglaciation 21–9 thousand years before present (version 1) – PMIP4 Core
551 experiment design and boundary conditions, *Geosci. Model Dev.*, 9, 2563-2587, <https://doi.org/10.5194/gmd-9-2563-2016>,
552 2016.

553



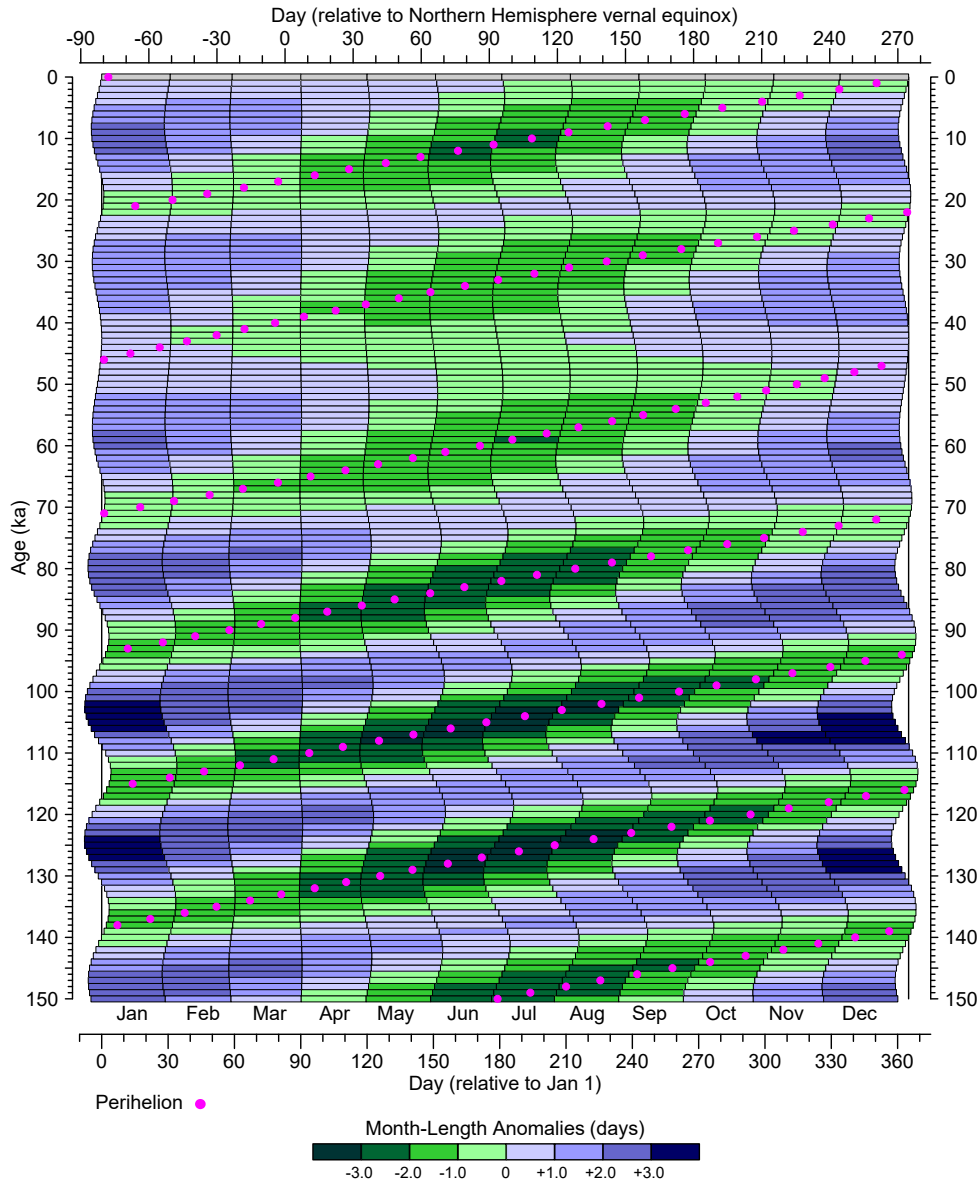
- 554 Izumi, K., Bartlein, P. J., and Harrison, S. P.: Consistent large-scale temperature responses in warm and cold climates,
555 Geophys. Res. Lett., 40, 1817-1823, <https://doi.org/10.1002/grl.50350>, 2013.
- 556
- 557 Joussaume, S. and Braconnot, P.: Sensitivity of paleoclimate simulation results to season definitions, J. Geophys. Res.-Atmos.,
558 102, 1943-1956, <https://doi.org/10.1029/96JD01989>, 1997.
- 559
- 560 Jungclauss, J., Giorgetta, M. A., Reick, C. H., Legutke, S., Brovkin, V., Crueger, T., Esch, M., Fieg, K., Fischer, N., Glushak,
561 K., Gayler, V., Haak, H., Hollweg, H.-D., Kinne, S., Kornblueh, L., Matei, D., Mauritsen, T., Mikolajewicz, U., Mueller, W.,
562 Notz, D., Pohlman, T., Raddatz, T., Rast, S., Roeckner, E., Saltzman, M., Schmidt, H., Schnur, R., Segschneider, J., Six, K.
563 D., Stockhause, M., Wegner, J., Widmann, H., Wieners, K.-H., Claussen, M., Marotzke, J., and Stevens, B.: CMIP5
564 simulations of the Max Planck Institute for Meteorology (MPI-M) based on the MPI-ESM-P model: The midHolocene
565 experiment, served by ESGF, WDCC at DKRZ, <http://dx.doi.org/10.1594/WDCC/CMIP5.MXEPmh>, 2012.
- 566
- 567 Kageyama, M., Braconnot, P., Harrison, S. P., Haywood, A. M., Jungclauss, J. H., Otto-Bliesner, B. L., Peterschmitt, J. Y.,
568 Abe-Ouchi, A., Albani, S., Bartlein, P. J., Brierley, C., Crucifix, M., Dolan, A., Fernandez-Donado, L., Fischer, H., Hoperft,
569 P. O., Ivanovic, R. F., Lambert, F., Lunt, D. J., Mahowald, N. M., Peltier, W. R., Phipps, S. J., Roche, D. M., Schmidt, G. A.,
570 Tarasov, L., Valdes, P. J., Zhang, Q., and Zhou, T.: The PMIP4 contribution to CMIP6 – Part 1: Overview and over-arching
571 analysis plan, Geosci. Model Dev., 11, 1033-1057, <https://doi.org/10.5194/gmd-11-1033-2018>, 2018.
- 572
- 573 Kutzbach, J. E. and Gallimore, R. G.: Sensitivity of a coupled atmosphere/mixed layer ocean model to changes in orbital
574 forcing at 9000 years B.P., J. Geophys. Res.-Atmos., 93, 803-821, <https://doi.org/10.1029/JD093iD01p00803>, 1988.
- 575
- 576 Kutzbach, J. E. and Otto-Bliesner, B. L.: The sensitivity of the African-Asian monsoonal climate to orbital parameter changes
577 for 9000 years B.P. in a low-resolution general circulation model, J. Atmos. Sci., 39, 1177-1188, [https://doi.org/10.1175/1520-0469\(1982\)039<1177:TSOTAA>2.0.CO;2](https://doi.org/10.1175/1520-0469(1982)039<1177:TSOTAA>2.0.CO;2), 1982.
- 578
- 579
- 580 Liu, Z., Otto-Bliesner, B. L., He, F., Brady, E. C., Tomas, R., Clark, P. U., Carlson, A. E., Lynch-Stieglitz, J., Curry, W.,
581 Brook, E., Erickson, D., Jacob, R., Kutzbach, J., and Cheng, J.: Transient simulation of last deglaciation with a new mechanism
582 for Bølling-Allerød warming, Science, 325, 310-314, <https://doi.org/10.1126/science.1171041>, 2009.
- 583
- 584 Marsicek, J., Shuman, B. N., Bartlein, P. J., Shafer, S. L., and Brewer, S.: Reconciling divergent trends and millennial
585 variations in Holocene temperatures, Nature, 554, 92, <https://doi.org/10.1038/nature25464>, 2018.
- 586



- 587 Otto-Bliesner, B., CCSM4 coupled simulation for CMIP5 with mid-Holocene conditions, served by ESGF, WDCC at DKRZ,
588 <http://dx.doi.org/10.1594/WDCC/CMIP5.NRS4mh>, 2014.
- 589
- 590 Otto-Bliesner, B. L., Braconnot, P., Harrison, S. P., Lunt, D. J., Abe-Ouchi, A., Albani, S., Bartlein, P. J., Capron, E., Carlson,
591 A. E., Dutton, A., Fischer, H., Goelzer, H., Govin, A., Haywood, A., Joos, F., LeGrande, A. N., Lipscomb, W. H., Lohmann,
592 G., Mahowald, N., Nehrbass-Ahles, C., Pausata, F. S. R., Peterschmitt, J. Y., Phipps, S. J., Renssen, H., and Zhang, Q.: The
593 PMIP4 contribution to CMIP6 – Part 2: Two interglacials, scientific objective and experimental design for Holocene and Last
594 Interglacial simulations, *Geosci. Model Dev.*, 10, 3979-4003, <https://doi.org/10.5194/gmd-10-3979-2017>, 2017.
- 595
- 596 Pollard, D. and Reusch, D. B.: A calendar conversion method for monthly mean paleoclimate model output with orbital forcing,
597 *J. Geophys. Res.-Atmos.*, 107, ACL 3-1-ACL 3-7, <https://doi.org/10.1029/2002JD002126>, 2002.
- 598
- 599 Saha, S., Moorthi, S., Pan, H.-L., Wu, X., Wang, J., Nadiga, S., Tripp, P., Kistler, R., Woollen, J., Behringer, D., Liu, H.,
600 Stokes, D., Grumbine, R., Gayno, G., Wang, J., Hou, Y.-T., Chuang, H.-y., Juang, H.-M. H., Sela, J., Iredell, M., Treadon, R.,
601 Kleist, D., Delst, P. V., Keyser, D., Derber, J., Ek, M., Meng, J., Wei, H., Yang, R., Lord, S., Dool, H. v. d., Kumar, A., Wang,
602 W., Long, C., Chelliah, M., Xue, Y., Huang, B., Schemm, J.-K., Ebisuzaki, W., Lin, R., Xie, P., Chen, M., Zhou, S., Higgins,
603 W., Zou, C.-Z., Liu, Q., Chen, Y., Han, Y., Cucurull, L., Reynolds, R. W., Rutledge, G., and Goldberg, M.: The NCEP Climate
604 Forecast System Reanalysis, *B. Am. Meteorol. Soc.*, 91, 1015-1058, <https://doi.org/10.1175/2010BAMS3001.1>, 2010.
- 605
- 606 Sénési, S., Richon, J., Franchistéguy, L., Tyteca, S., Moine, M.-P., Voldoire, A., Sanchez-Gomez, E., Salas y Mélia, D.,
607 Decharme, B., Cassou, C., Valcke, S., Beau, I., Alias, A., Chevallier, M., Déqué, M., Deshayes, J., Douville, H., Madec, G.,
608 Maisonnave, E., Planton, S., Saint-Martin, D., Szopa, S., Alkama, R., Belamari, S., Braun, A., Coquart, L., Chauvin, F., CNRM-
609 CM5 model output prepared for CMIP5 midHolocene, served by ESGF, WDCC at DKRZ,
610 <http://dx.doi.org/10.1594/WDCC/CMIP5.CEC5mh>, 2014.
- 611
- 612 Timm, O., Timmermann, A., Abe-Ouchi, A., Saito, F., and Segawa, T.: On the definition of seasons in paleoclimate simulations
613 with orbital forcing, *Paleoceanography*, 23, <https://doi.org/10.1029/2007PA001461>, 2008.
- 614
- 615 Xie, P. and Arkin, P. A.: Global precipitation: A 17-year monthly analysis based on gauge observations, satellite estimates,
616 and numerical model outputs, *B. Am. Meteorol. Soc.*, 78, 2539-2558, [https://doi.org/10.1175/1520-0477\(1997\)078<2539:GPAYMA>2.0.CO;2](https://doi.org/10.1175/1520-0477(1997)078<2539:GPAYMA>2.0.CO;2), 1997.
- 617



618

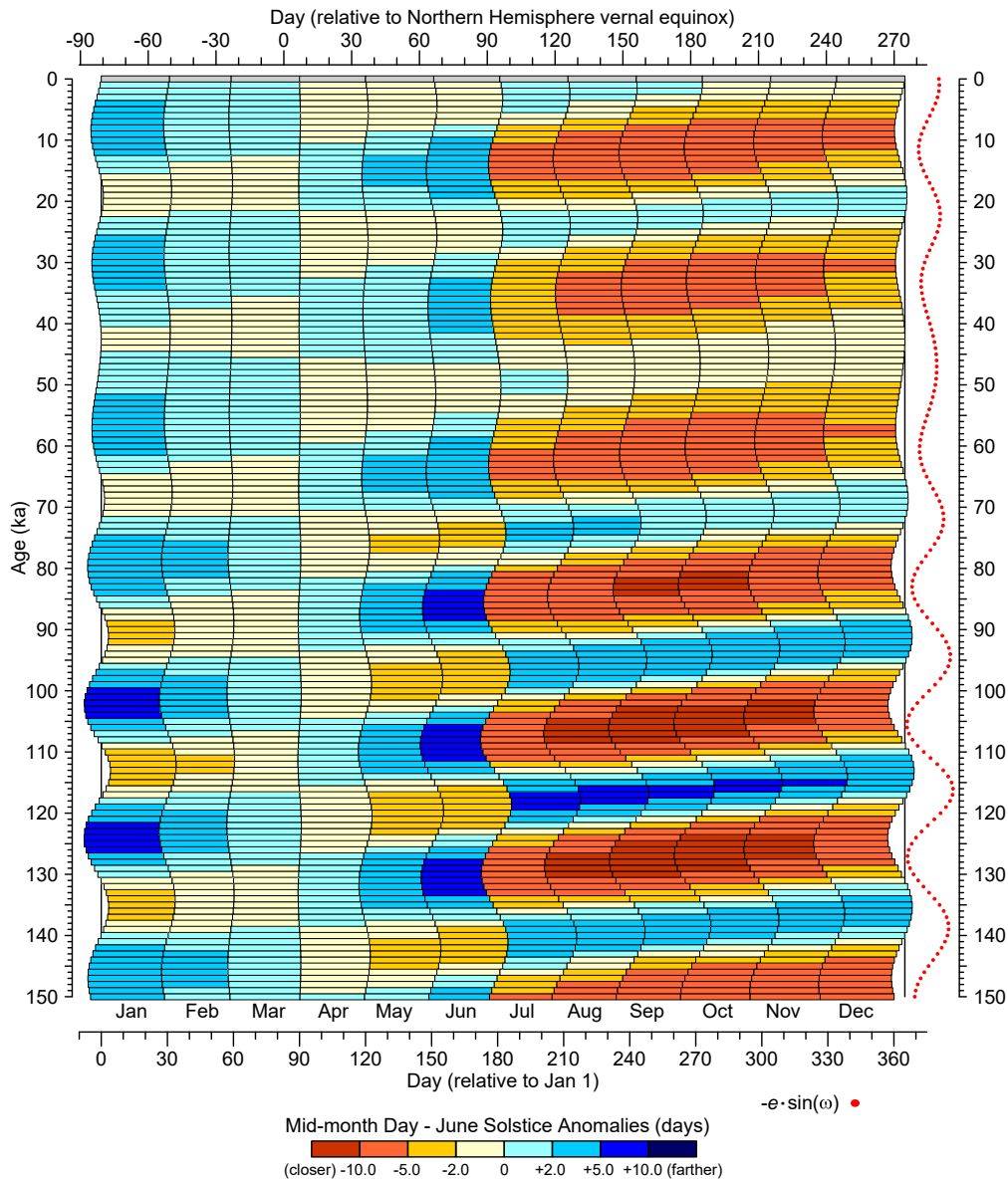


619

620 **Figure 1.** Variations over the past 150 kyr in the beginning and ending days of fixed-angular months for a 365-day "noleap" calendar, shown
 621 for 1 kyr intervals beginning at 0 ka (1950 CE). The left side of each horizontal bar shows the beginning day while the right side shows the
 622 ending day of a particular month for each 1 kyr interval. The month-length "anomalies" or differences from the present-day are shown by
 623 shading, with individual paleo months that are shorter than those at present indicated by green shades and those that are longer indicated by
 624 blue shades. The day that perihelion occurs for each 1 kyr interval is indicated by a magenta dot, and the overall pattern of month-length
 625 anomalies can be seen to follow the day of perihelion. The figure shows that the changing month lengths move the beginning, middle and
 626 ending days of each month (as well as the beginning and ending days of the year).



627

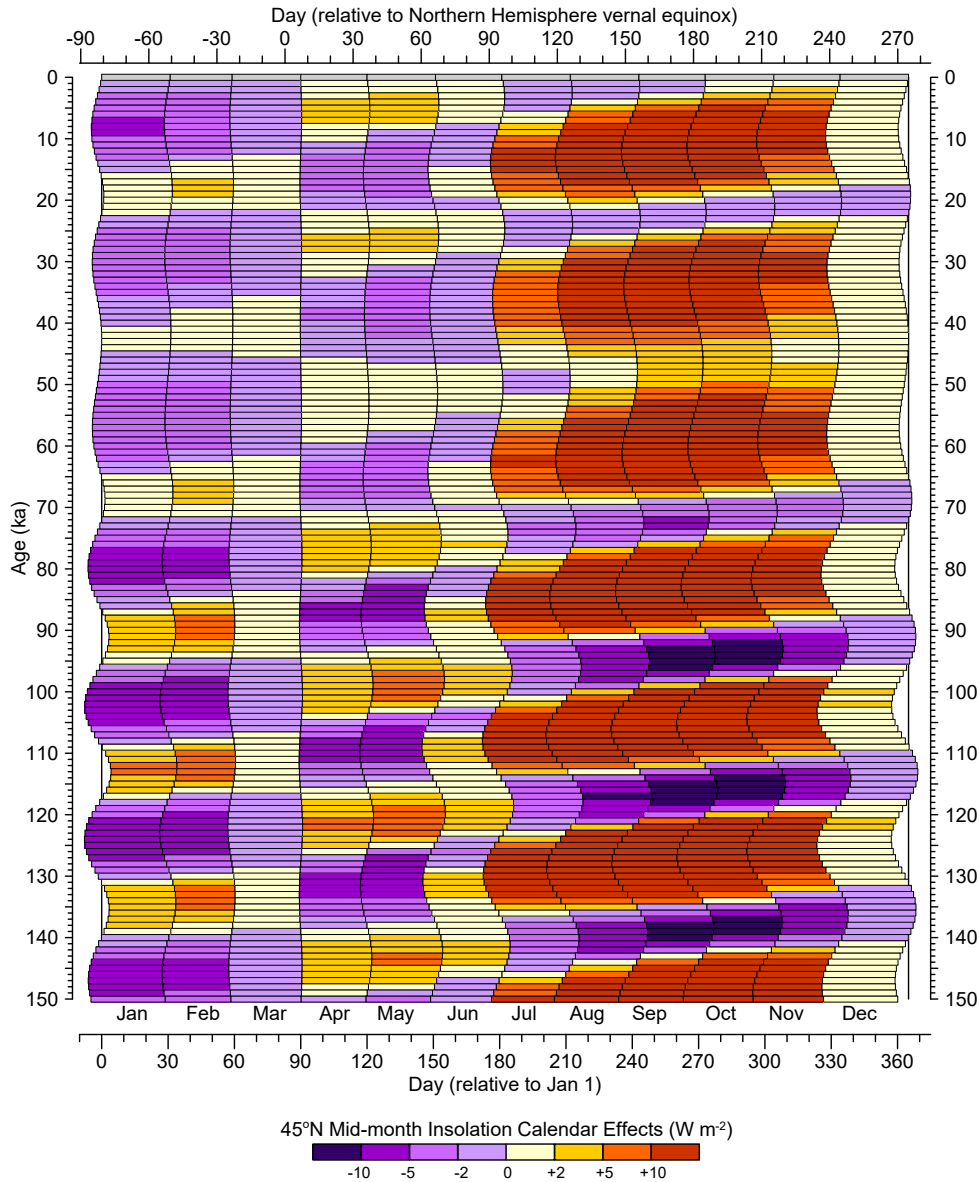


628

629 **Figure 2.** Variations in the difference (in days) between the mid-month day of each month and the day of the June solstice. Months that are
 630 shifted closer to the June solstice are indicated by orange hues while those that are farther away are indicated by blue. As in Fig. 1, variations
 631 over the past 150 kyr in the beginning and ending days of fixed-angular months for a 365-day "noleap" calendar are shown for 1 kyr intervals
 632 beginning at 0 ka (1950 CE). The left side of each horizontal bar shows the beginning day while the right side shows the ending day of a
 633 particular month for each 1 kyr interval. Variations in the beginning and ending days of individual months can be seen to track the climatic
 634 precession parameter ($e \cdot \sin \omega$, where e is eccentricity and ω is the longitude of perihelion measured from the vernal equinox, an index of
 635 Earth's distance from the Sun at the summer solstice), which is plotted at the right side of the figure (red dots). (Note that the inverse of the
 636 climatic precession parameter is plotted for easier comparison.)



637



638

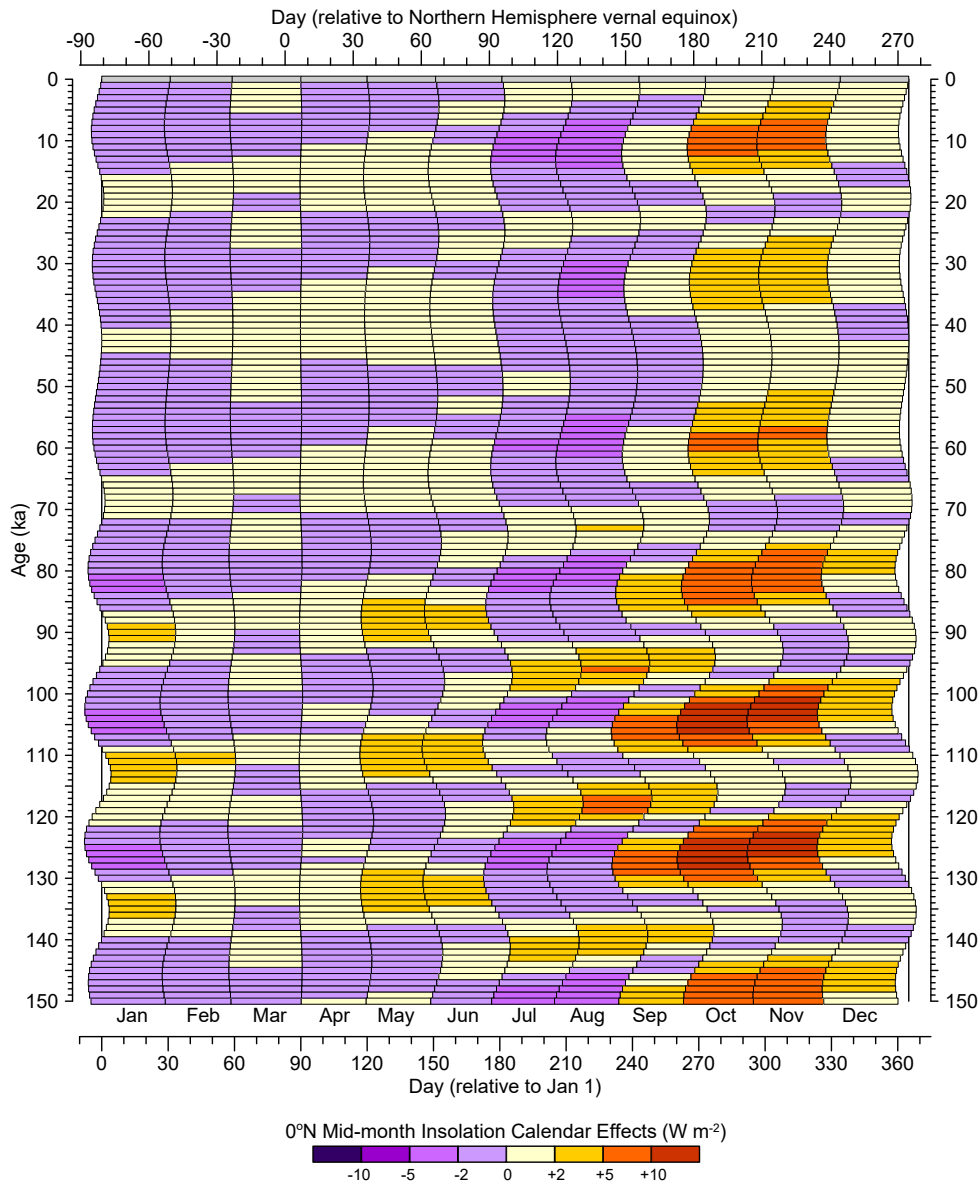
639 **Figure 3.** Calendar effects on insolation at 45° N. The differences plotted show the values of average daily insolation at mid-month days
640 identified using the appropriate fixed-angular paleo calendar minus those using the fixed-length definition of present-day months, with
641 orange hues showing positive difference, and purple hues negative. As in Fig. 1, variations over the past 150 kyr in the beginning and ending
642 days of fixed-angular months for a 365-day "no-leap" calendar are shown for 1 kyr intervals beginning at 0 ka (1950 CE). The left side of
643 each horizontal bar shows the beginning day while the right side shows the ending day of a particular month for each 1 kyr interval.

644



645

646

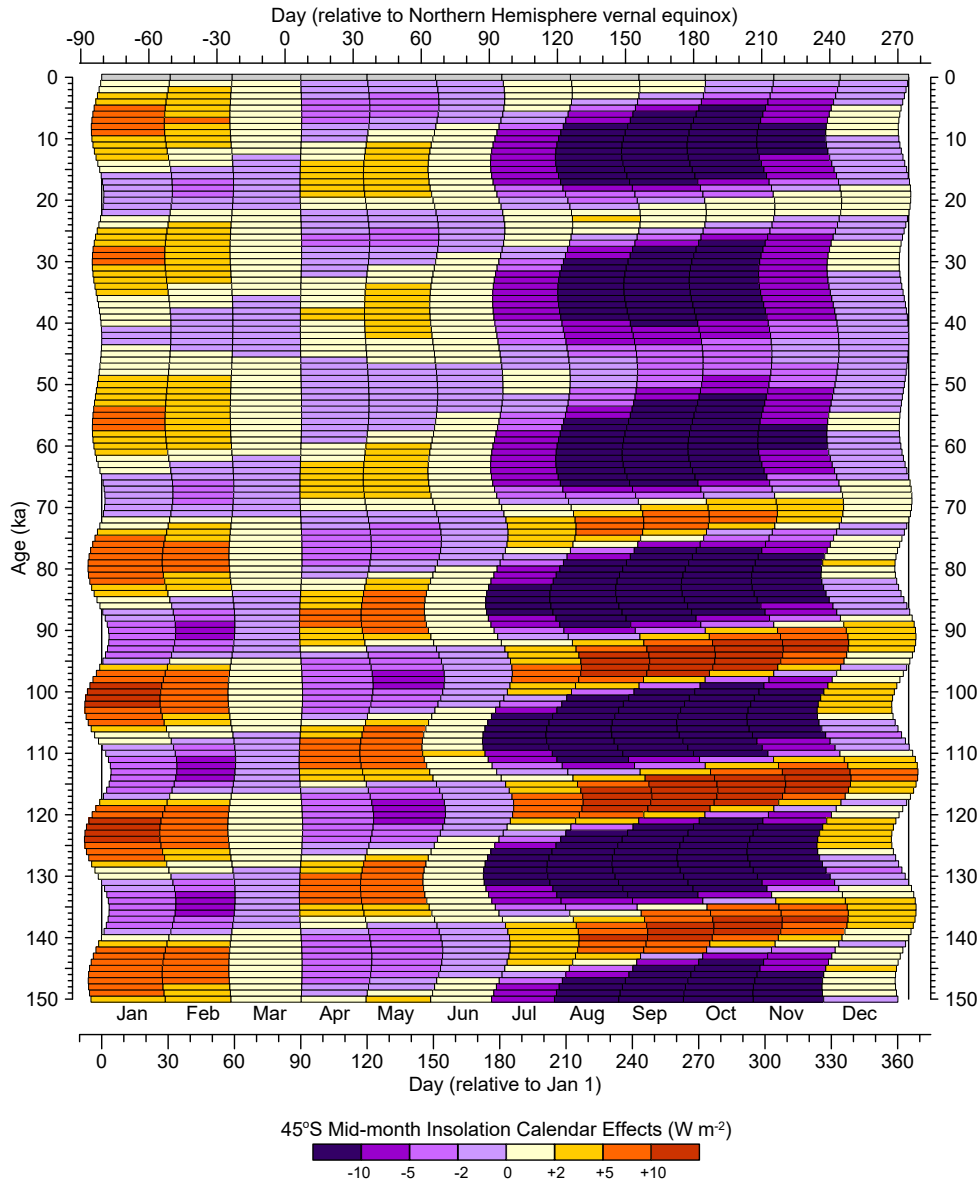


647

648 **Figure 4.** Calendar effects on insolation at the equator. The differences plotted show the values of average daily insolation at mid-month
649 days identified using the appropriate fixed-angular paleo calendar minus those using the fixed-length definition of present-day months, with
650 orange hues showing positive difference, and purple hues negative. As in Fig. 1, variations over the past 150 kyr in the beginning and ending
651 days of fixed-angular months for a 365-day "no-leap" calendar are shown for 1 kyr intervals beginning at 0 ka (1950 CE). The left side of
652 each horizontal bar shows the beginning day while the right side shows the ending day of a particular month for each 1 kyr interval.



653



654

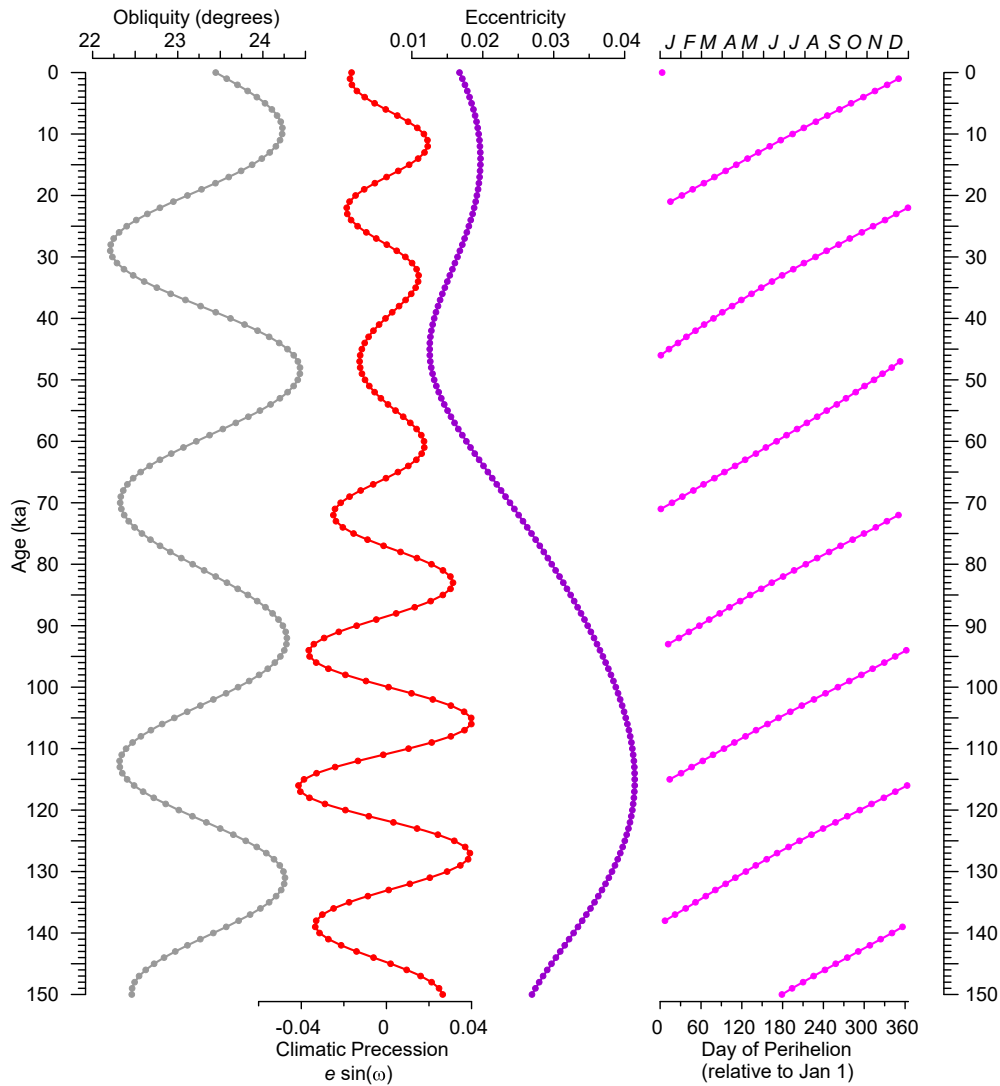
655 **Figure 5.** Calendar effects on insolation at 45° S. The differences plotted show the values of average daily insolation at mid-month days
 656 identified using the appropriate fixed-angular paleo calendar minus those using the fixed-length definition of present-day months, with
 657 orange hues showing positive difference, and purple hues negative difference. As in Fig. 1, variations over the past 150 kyr in the beginning
 658 and ending days of fixed-angular months for a 365-day "noleap" calendar are shown for 1 kyr intervals beginning at 0 ka (1950 CE). The
 659 left side of each horizontal bar shows the beginning day while the right side shows the ending day of a particular month for each 1 kyr
 660 interval.

661



662

663

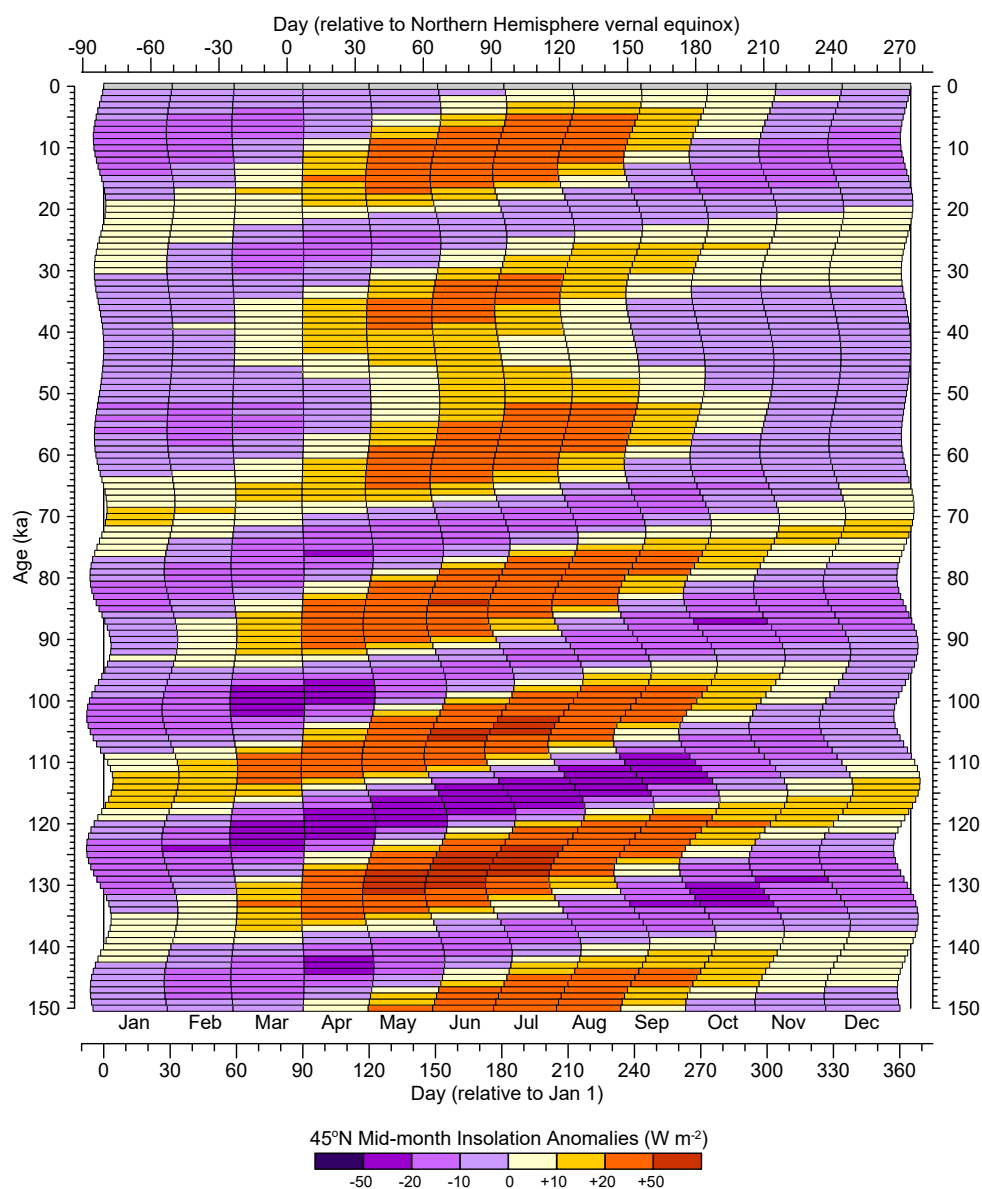


664

665 **Figure 6.** Orbital parameter variations at 1 kyr intervals over the past 150 kyr for obliquity, climatic precession, eccentricity, and day of
 666 perihelion (relative to January 1). Climatic precession is calculated as $e \cdot \sin(\omega)$, where e is eccentricity and ω is the longitude of perihelion
 667 measured from the vernal equinox.

668

669

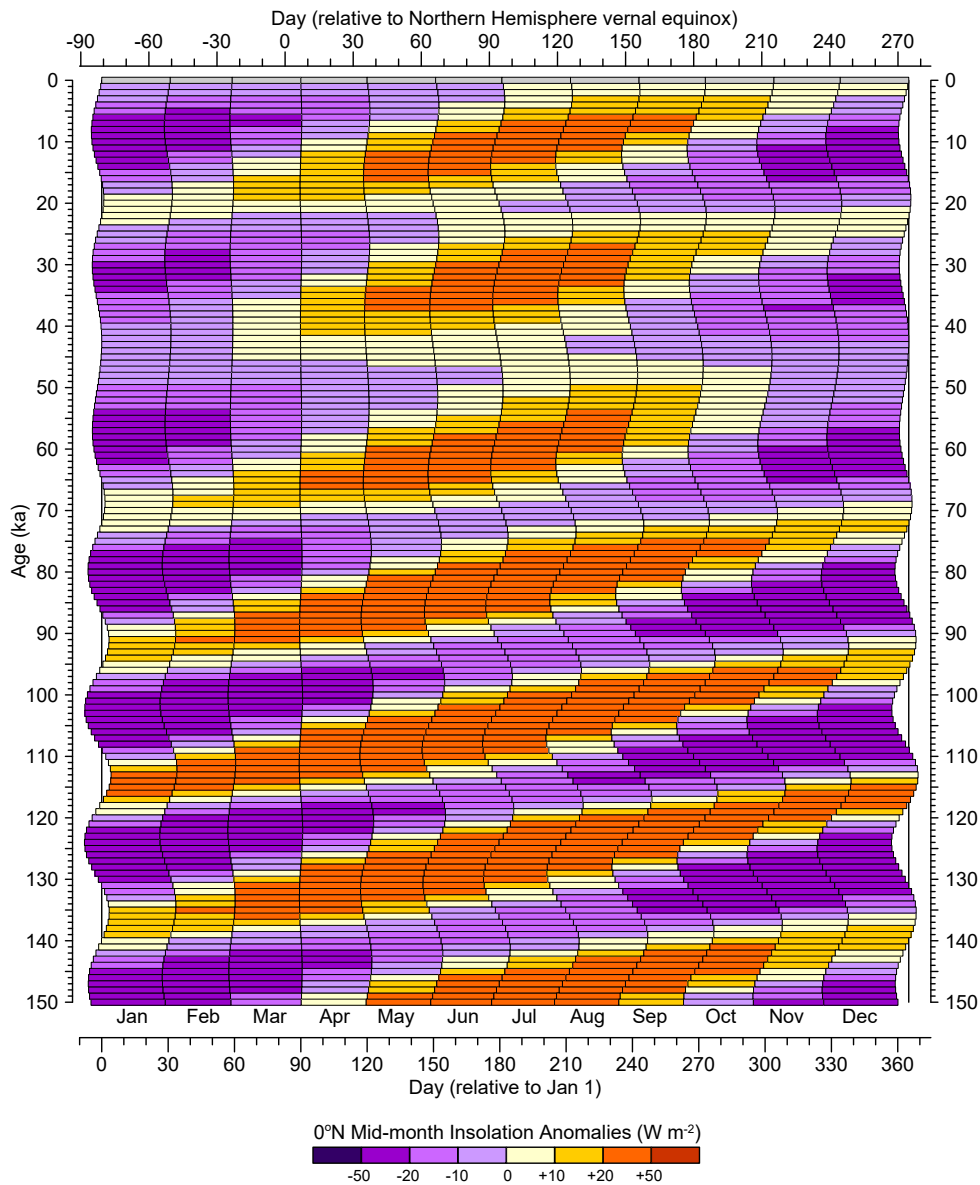


670

671 **Figure 7.** Long-term differences in mid-month average daily insolation relative to present (0 ka or 1950 CE) at 45° N for a fixed-angular
 672 calendar. As in Fig. 1, variations over the past 150 kyr in the beginning and ending days of fixed-angular months for a 365-day "no-leap"
 673 calendar are shown for 1 kyr intervals beginning at 0 ka (1950 CE). The left side of each horizontal bar shows the beginning day while the
 674 right side shows the ending day of a particular month for each 1 kyr interval.

675

676

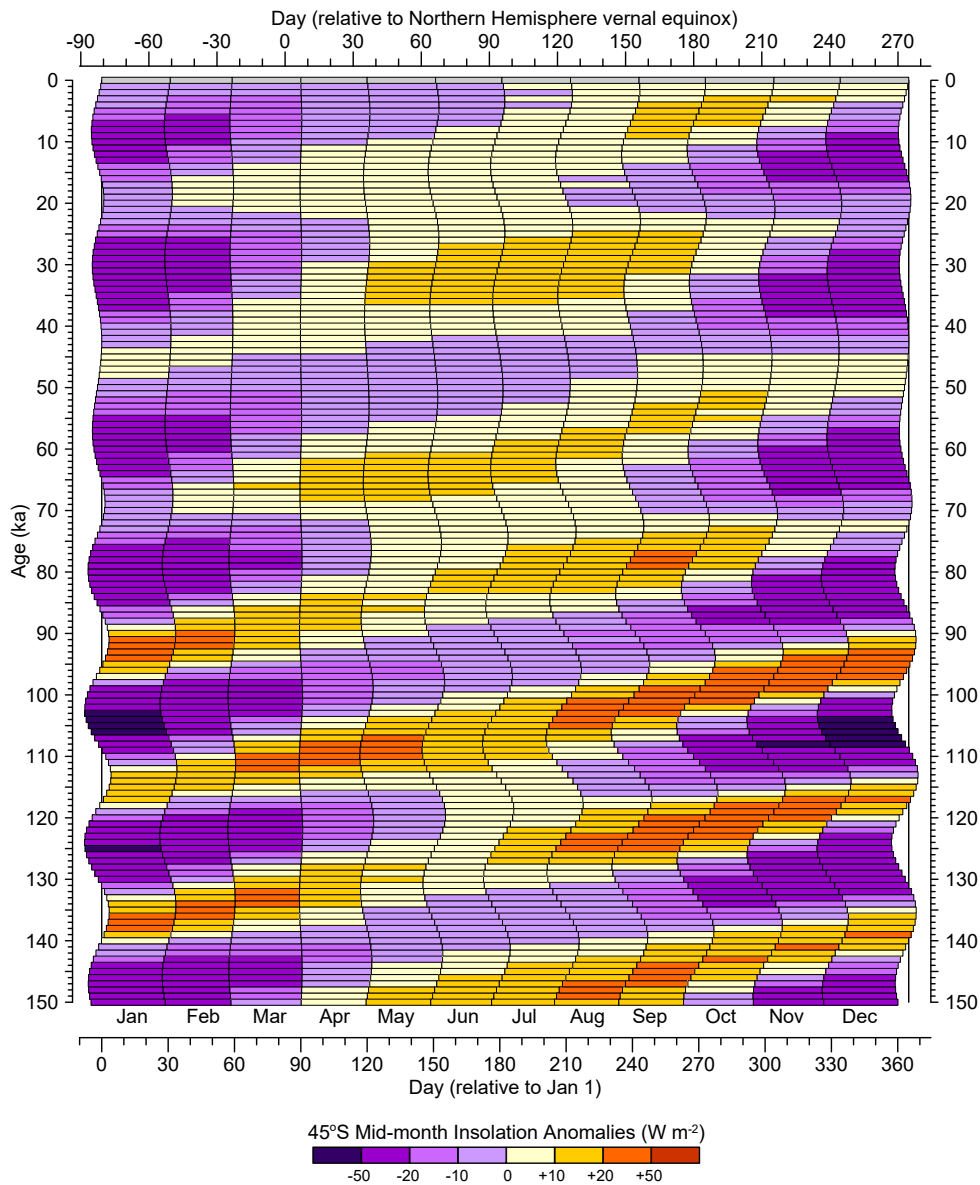


677

678 **Figure 8.** Long-term differences in mid-month average daily insolation relative to present (0 ka or 1950 CE) at the equator for a fixed-
679 angular calendar. As in Fig. 1, variations over the past 150 kyr in the beginning and ending days of fixed-angular months for a 365-day
680 "no-leap" calendar are shown for 1 kyr intervals beginning at 0 ka (1950 CE). The left side of each horizontal bar shows the beginning day
681 while the right side shows the ending day of a particular month for each 1 kyr interval.

682

683



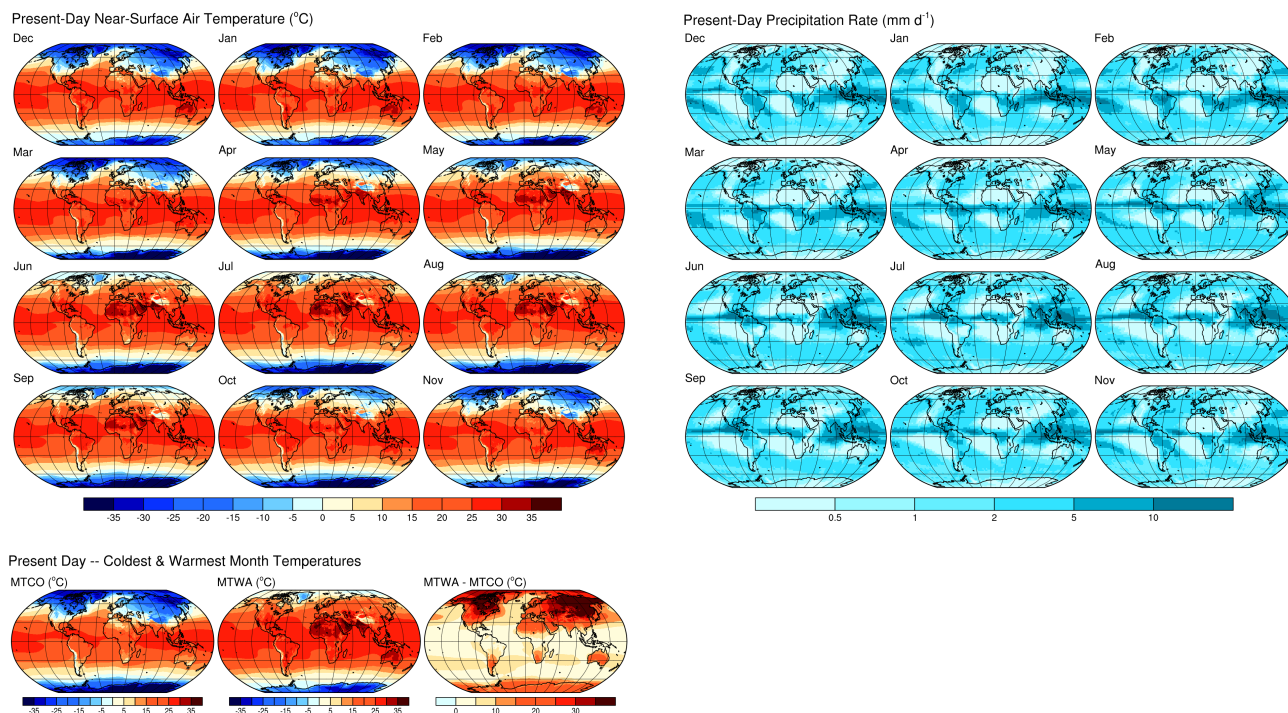
684

685 **Figure 9.** Long-term differences in mid-month average daily insolation relative to present (0 ka or 1950 CE) at 45° S for a fixed-angular
686 calendar. As in Fig. 1, variations over the past 150 kyr in the beginning and ending days of fixed-angular months for a 365-day "noleap"
687 calendar are shown for 1 kyr intervals beginning at 0 ka (1950 CE). The left side of each horizontal bar shows the beginning day while the
688 right side shows the ending day of a particular month for each 1 kyr interval.

689

690

691



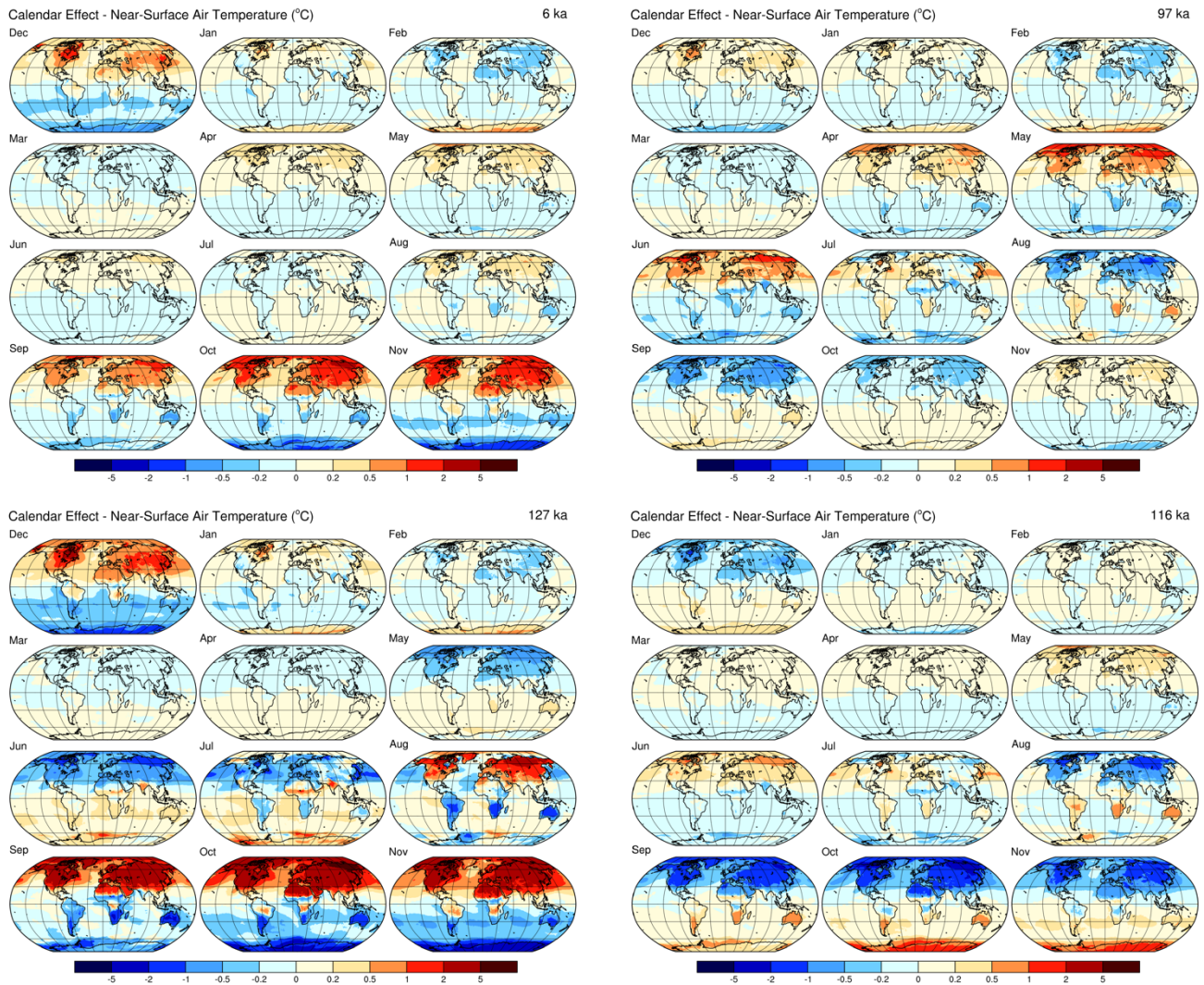
692

693 **Figure 10.** Present-day (1981-2010 CE) long-term mean values of monthly near-surface air temperature (*tas*) from the Climate Forecast
694 System Reanalysis (CFSR), the mean temperatures of the warmest and coldest months and their differences from the same data, and
695 precipitation rate (*precip*) from the CPC Merged Analysis of Precipitation (CMAP).

696

697

698



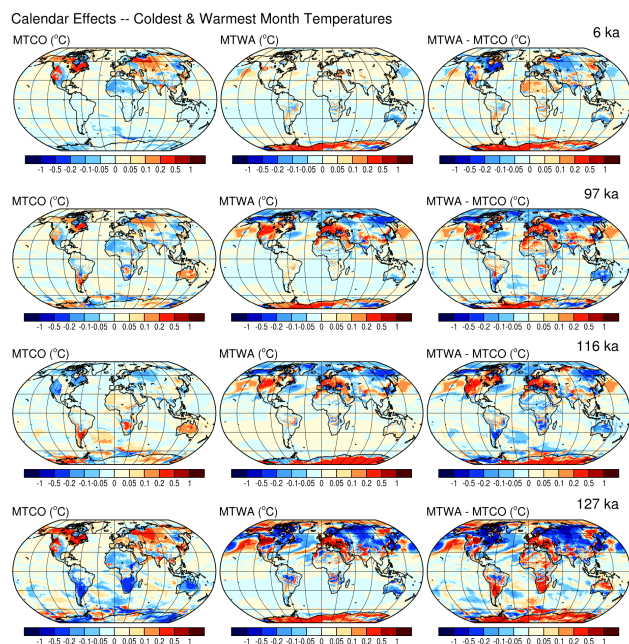
699

700 **Figure 11.** Calendar effects on near-surface air temperature for 6 ka (upper left), 97 ka (upper right), 127 ka (lower left) and 116 ka (lower
701 right). The maps show the patterns of month-length adjusted average temperatures minus the unadjusted values, using 1981-2010 long-term
702 averages of CFSR *tas* values, with positive difference (indicating that the adjusted data would be warmer than unadjusted data) in red hues,
703 and negative differences in blue.

704



705



706

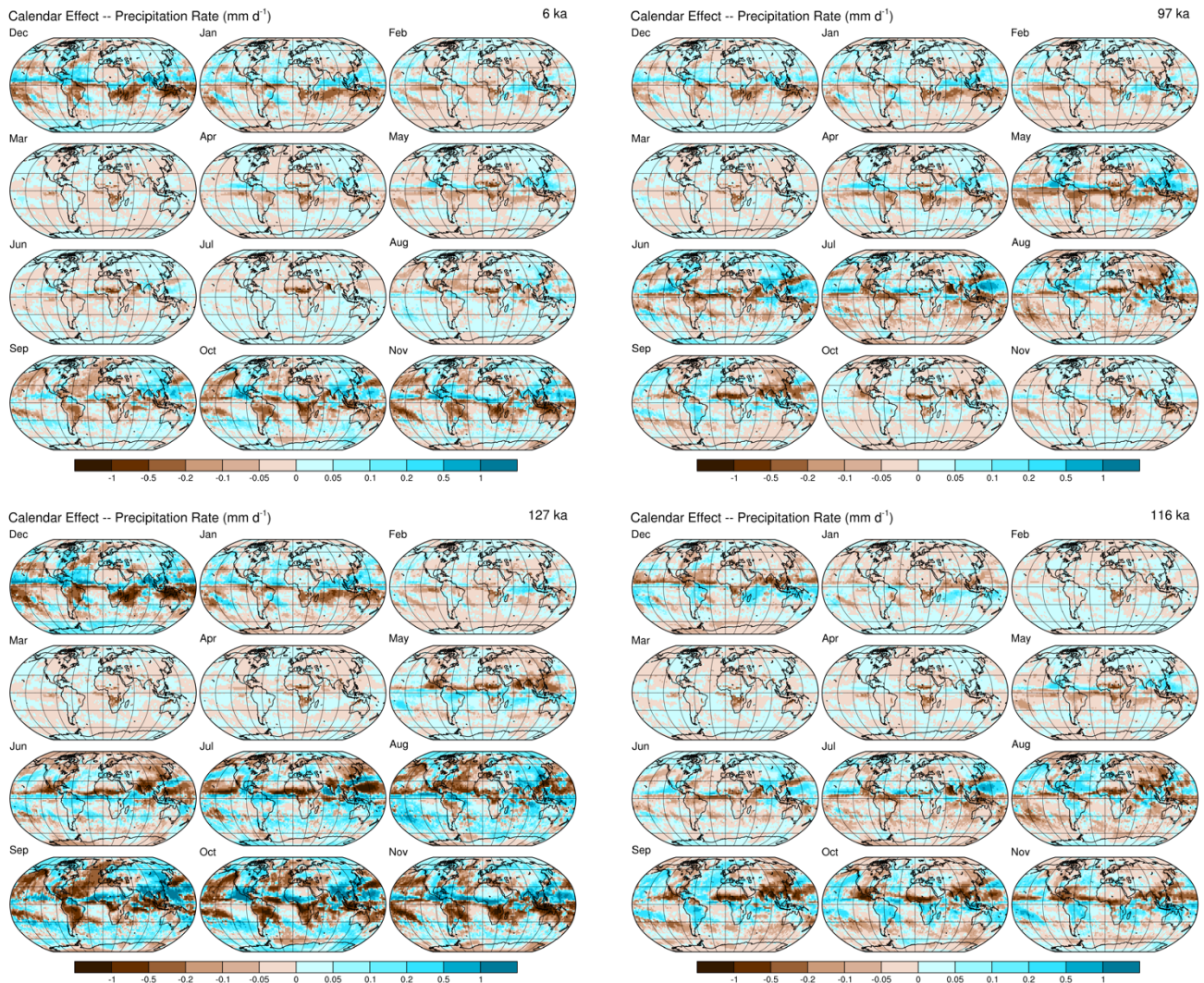
707 **Figure 12.** Calendar effects on the mean near-surface air temperatures of the warmest (MTWA) and coldest (MTCO) months and their
 708 differences (an index of seasonality) for 6 ka, 97 ka, 116 ka and 127 ka (top to bottom row). The maps show the patterns of month-length
 709 adjusted average temperatures minus the unadjusted values for MTWA and MTCO, using 1981-2010 long-term averages of CFSR *tas* values,
 710 with positive difference (indicating that the adjusted data would be warmer than unadjusted data) in red hues, and negative differences in
 711 blue.

712

713



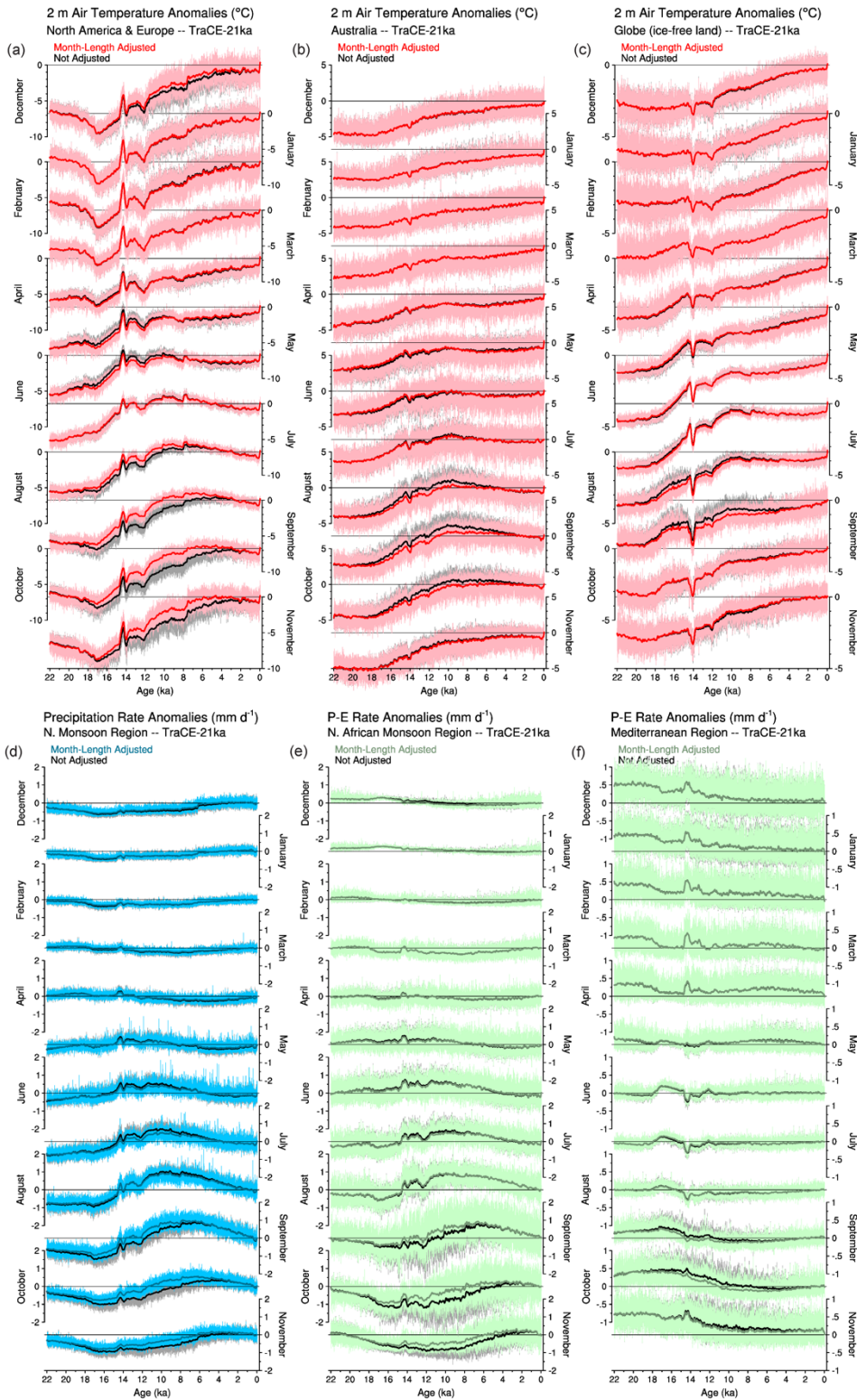
714



715

716 **Figure 13.** Calendar effects on precipitation rate for 6 ka (upper left), 97 ka (upper right), 127 ka (lower left) and 116 ka (lower right). The
717 maps show the patterns of month-length adjusted precipitation rate minus the unadjusted values, using 1981-2010 long-term averages of
718 CMAP *precip* values, with positive difference (indicating that the adjusted data would be wetter than unadjusted data) in blue hues, and
719 negative differences in brown.

720

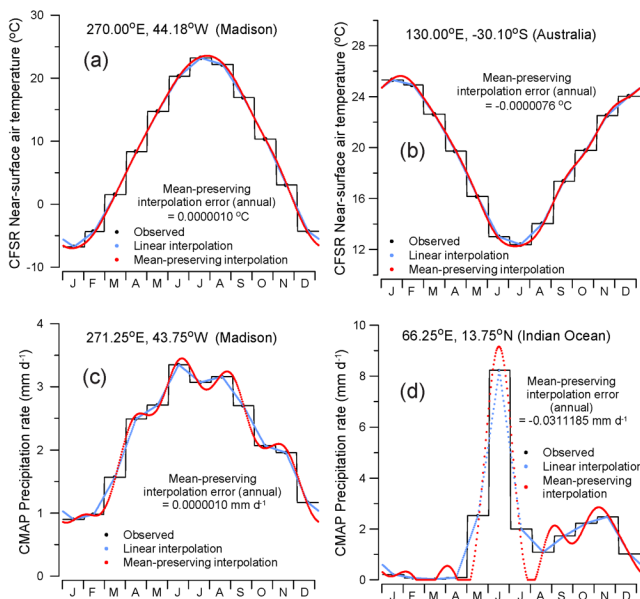




722 **Figure 14.** Time series of original and month-length-adjusted annual area-weighted averages of TraCE-21k data (Liu et al., 2009), expressed
 723 as difference from the 1961-1989 long-term mean for (a-c) 2 m air temperature, (d) precipitation rate, and (e-f) precipitation minus
 724 evaporation (P - E). The original or unadjusted data are plotted in gray and black, and the adjusted data in colors. The area averages are grid-
 725 cell area-weighted values for land grid points in each region, and the smoother curves are locally weighted regression curves with a window
 726 half-width of 100 years. The regions are defined as: (a) 15 to 75° N and -170 to 60° E, (b) 10 to 50° S and 110 to 160° E, (c) global ice-free
 727 land area, (d) 0 to 30° N and -30 to 120° E, (e) 5 to 17° N and -5 to 30° E, and (f) 31 to 43° N and -5 to 30° E.

728

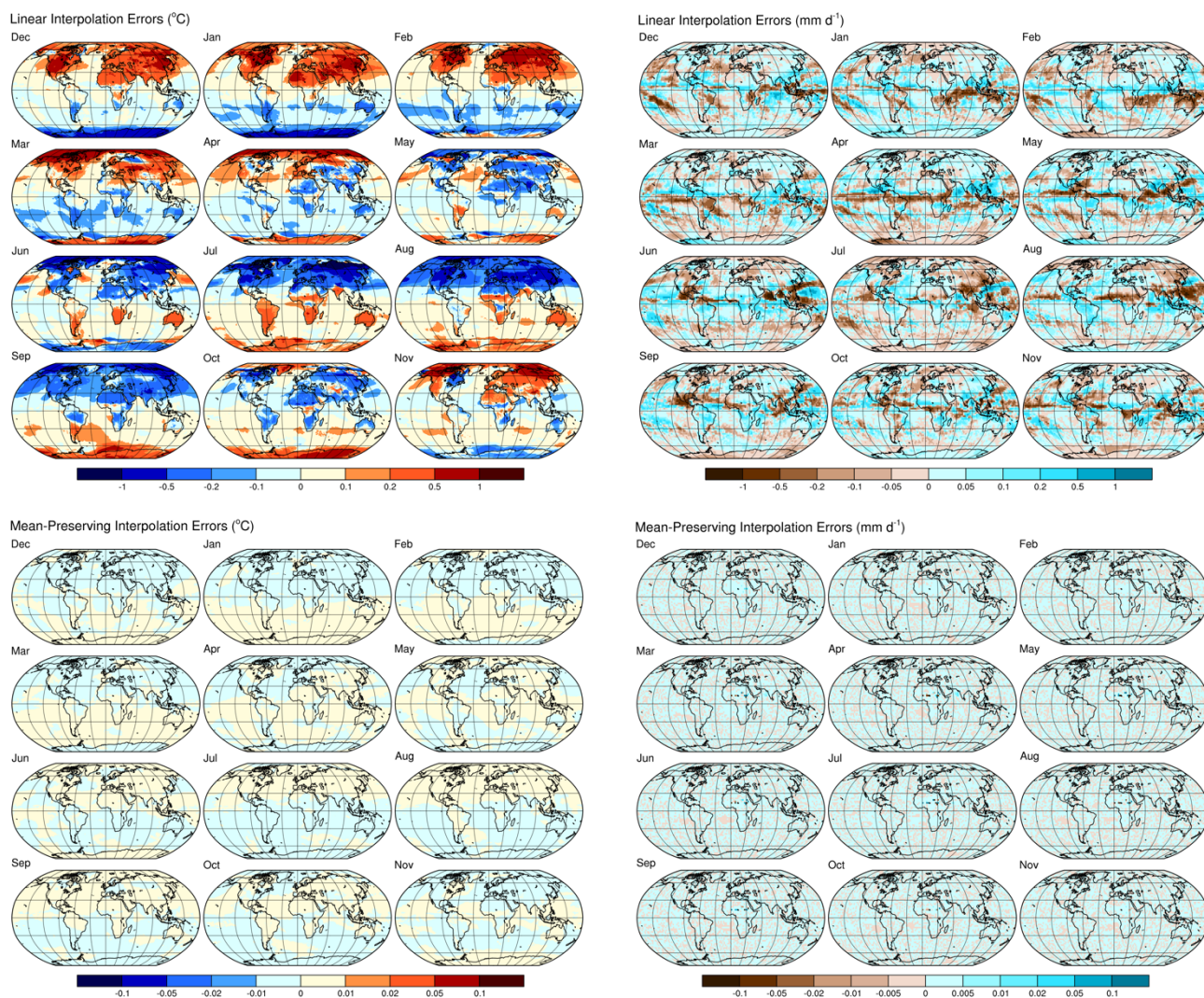
729



730

731 **Figure 15.** Pseudo-daily interpolated temperature (top row) and precipitation (bottom row) for some representative locations: (a, c) Madison,
 732 Wisconsin, USA, (b) Australia, and (d) the Indian Ocean. The original monthly mean data are shown by the black dots and stepped curves
 733 (black lines), daily values linearly interpolated between the monthly mean values are shown in blue, and daily values using the mean-
 734 preserving approach of Epstein (1991) are shown in red. The annual interpolation error (or the difference between the annual average
 735 calculated using the original data and the pseudo-daily interpolated data) is given for the mean-preserving approach in each case. The
 736 interpolated data for this figure were generated using the program `demo_01_pseudo_daily_interp.f90`.

737



738

739 **Figure 16.** Pseudo-daily interpolation errors for CFSR near-surface air temperature (left-hand column) and CMAP precipitation rate (right-
740 hand column). The top set of maps shows the interpolation errors, or the differences between the original monthly mean values and the
741 monthly mean values recalculated from linear interpolation of pseudo-daily values. The bottom set of maps shows the interpolation errors
742 for mean-preserving (Epstein, 1991) interpolation.

743

744